SPE 141596

Domain Decomposition Methods Applied to Coupled Flow-Geomechanics Reservoir Simulation

Horacio Florez, UT-Austin; Mary Wheeler, SPE, UT-Austin; Adolfo A. Rodriguez, SPE, ConocoPhillips; Jorge E.P. Monteagudo, SPE, ConocoPhillips

This paper was prepared for presentation at the SPE Reservoir Simulation Symposium held in The Woodlands, Texas, USA, 21–23 February 2011.

Abstract

In this work, well established Domain Decomposition techniques have been studied in order to carry out efficient simulations of coupled flow/geomechanics problems by taking full advantage of current parallel computer architectures. Different solution schemes can be defined depending upon transmission conditions among sub-domain interfaces. Three different schemes, i.e. Dirichlet-Neumann, Neumann-Neumann and Mortar-FEM, are tested and the advantages and disadvantages of each of them identified. This work will focus in the coupling of different meshes and/or physics on different domains by means of the Mortar-FEM plus the above DD-Schemes. Several examples of coupling of elasticity and poroelasticity in the context of reservoir compaction and subsidence are presented. In order to facilitate the implementation of complex workflows, we have implemented an advanced Python wrapper interface that allows programming capabilities. We have applied this platform to a variety of problems ranging from near-wellbore applications to field level subsidence calculations.

Introduction

Hydrocarbon production or the injection of fluids in the reservoir can produce changes in the rock stresses and in-situ geomechanics, potentially leading to compaction and subsidence with harmful effects in wells, cap-rock, faults, and the surrounding environment as well. In order to predict these changes and their impact, accurate simulations are essential. In many cases, the flow simulation needs to be coupled to geomechanics causing a significant increase in CPU time and memory requirements (Dean et al., 2006; Gai, 2004).

Geomechanical aspects are important for the oil and gas industry due to their impact to the environment and to production operations. At the reservoir level, subsidence on surface due to reservoir compaction may be an important issue for the surrounding environment and it may put on risk the production facilities because large deformation might occur. One can also look at reservoir compaction as a secondary recovery mechanism in the sense that additional hydrocarbons might be extracted because of the deformations induced by the pressure drop. At the well level, i.e. near borehole geomechanics, borehole stability issues during drilling and sand production may become a major problem in the day-to-day operations.

It is well known that in coupled flow-geomechanic simulations, the geomechanics component can take as much as 90% of the total CPU. In order to overcome the CPU burden associated to mechanic calculations, Domain Decomposition (DD) techniques have been subject to intensive study. DD entails the partitioning of the domain in a set of sub-domains in a way that each can be solved separately in order to exploit parallel computer architectures. The splitting of the global problems into pieces provides some degree of parallelism with the resulting speed-up compared against a serial or sequential simulation. This allows us to tackle larger and more complicated problems as well as reducing the overall computational time. DD-schemes also allow having different physics and different meshes on different domains, i.e. non-conforming meshes or hanging nodes. This capability is attractive for coupled flow and geomechanics simulations where one wants to couple poroelasticity in the pay-zone with elasticity in the surroundings, or even poroplasticity in some layers of the reservoir with elasticity elsewhere.

The work done by Gutierrez and Lewis (Gutierrez et al., 2001) recognized the increasing role of geomechanics in petroleum reservoir engineering as deeper formations are explored and exploited. For instance, stresses, fluid pressure and temperature conditions found at large depths may lead to a range of situations where conventional reservoir modeling fails to provide an

accurate analysis (Charlez, 1999; Longuemare et al., 2002; Pao et al., 2001).

Poroelasticity is the basic theory to predict the compaction of a producing hydrocarbon reservoir and the related hazards, including land subsidence and borehole damages (Pao et al., 2001; Yin et al., 2009). Several environmental issues connected with ground-water withdrawal, or the safe long-term disposal of wastes in the subsurface, i.e. issues related to radioactive waste repository design and performance, can be addressed with the aid of poroelastic models (Ferronato et al., 2010). Modeling of offshore reservoirs near salt bodies can also be modeled effectively in this way (Minkoff et al., 2003).

Poroelasticity describes the coupled process between mechanics and flow in porous media. Its theoretical basis goes back to the mid 1920s when Terzaghi described analytically the one-dimensional consolidation of a soil column under a constant load (Terzaghi, 1923, 1943). Biot (Biot, 1941) developed the first three-dimensional coupled poroelastic system to describe the dynamics of porous media with the coupling between the fluid flow and the stress. This pioneering work is a basic isothermal theory with saturated single phase flow inside solid matrix, which is based on a linear stress-strain constitutive relationship and a linear form of Darcy's flow law. An important reformulation of Biot's theory was done by Rice and Cleary (Rice and Cleary, 1976). They formulated the equations by using material coefficients which are more concise and easier to use in practical applications (Liu, 2004). Other more sophisticated approaches have been recently proposed, i.e. (Coussy, 2004), however, Biot's remains the most popular.

Direct applications of geomechanics to hydrocarbon reservoirs are relatively rare but can be tracked back to the early work of Geertsma (Geertsma, 1957, 1973), Gassman (Gassmann, 1951) and later, by others (Pao et al., 2001). In order to solve efficiently the poroelasticity governing equations the Finite Element Method have become the most popular tool for the mechanics calculation. For flow simulations Central Finite Differences schemes are still use in major reservoir simulators.

Lewis and Schrefler (Lewis and Schrefler, 1998) presented and applied such methods to one- and two-dimensional problems in consolidation and to the problem of subsidence in Venice. Other numerical works have been conducted at the Center for Subsurface Modeling, at the University of Texas at Austin. There, Liu (Liu, 2004) implemented a scheme involving Taylor–Hood elements and, subsequently, a DG variant based on the work of Phillips and Wheeler (Phillips and Wheeler, 2007a, b). Gai (Gai, 2004) used continuous elements for displacements and a cell-centered finite difference method for pressure, and implemented an iteratively coupled scheme to find the numerical solution. She also studied the multiphase flow version of the poroelasticity equations. Phillips and Wheeler (Phillips and Wheeler, 2007a, b) presented the theoretical convergence of two-dimensional (2-D) models that couple both continuous and discontinuous Galerkin elements for the displacements with mixed spaces for the fluid flow. In addition, Girault, Pencheva, Wheeler, and Wildey presented a domain decomposition method for solving linear elasticity. Their algorithm uses mortar spaces as displacement boundary conditions and was designed to eliminate rigid body motions. Information is transferred by jumps, and mortars are introduced at the interfaces to dissociate the computation between neighboring subdomains (Girault et al., 2009).

One of the first applications of the Continuous Galerkin Finite Element Method (CG-FEM) was published in 1969 by Sanhu and Wilson (Sandhu and Wilson, 1969). They applied a FEM formulation to three-dimensional soil consolidation problems which was later revisited by Yokoo (Muller et al., 2009; Santarelli et al., 1992). Fluid's compressibility was taken into account by Ghaboussi and Wilson (Belayneh, 2004). They briefly commented on the stability of CG schemes as well (Kim et al., 2009). Zienkiewicz et al. (Zienkiewicz et al., 1977) introduced the compressibility of the solid grains. The stability analysis in time was performed by Booker and Small (Booker and Small, 1987).

Zienkiewicz and Shiomi (Zienkiewicz and Shiomi, 1984) discussed various CG formulations for soil consolidation problems. Mixed finite elements (Phillips, 2005; Phillips and Wheeler, 2007a, b), reduced integrations (Souza-Neto et al., 2008), and penalty methods (Wheeler, 1978), which were studied and used for dealing with incompressible elasticity problems, were proposed for consolidation problems with incompressible fluid models. Multiple CG applications have been applied to various practical poromechanics problems. In particular, applications in the area of petroleum engineering can be found in (Chin et al., 2000; Dean et al., 2006; Settari and Walters, 2001; Shao, 1997).

Domain decomposition methods (DDM) are very efficient algorithms to compute the solution of large scale problems on parallel computers. These methods mainly consist of splitting the global domain into several subdomains and to compute the solution on the global domain through the resolution of the problem associated with each subdomain (Maday and Magoules, 2006). The theory for DDM can be found elsewhere (Quarteroni and Valli, 1999; Toselli and Widlund, 2004). However, for porous media problems, a DDM with optimal scalability has yet to be found (Ferronato et al., 2008; Girault et al., 2009; Turska and Schrefler, 1993; Turska et al., 1994).

In terms of coupling, several approaches are possible, the most common being loose or iterative coupling methods in which the two problems are solved in sequence (Gai, 2004).The monolithic approach, where all field equations are solved simultaneously, is regarded as the most suitable one (Bianco et al., 2003; Gawin et al., 1998) for this type of problems (Stavroulakis and Papadrakakis, 2009).

Mathematical Model

It can be shown that (Gai, 2004), for deformable porous media, the single-phase flow model derives from continuity equation for incompressible flow and Darcy's law yields:

$$\frac{\partial \varphi^*}{\partial t} + \nabla \cdot \left(-\frac{1}{\mu} \underline{\underline{\boldsymbol{K}}} \left(\nabla p - \rho g \nabla z \right) \right) = q \tag{1}$$

where φ^* is model specific porosity, $\underline{\underline{\boldsymbol{K}}}$ is the absolute permeability tensor, μ is the dynamic viscosity, ρ is the fluid density, $\boldsymbol{g}$ is the gravity acceleration constant, $\boldsymbol{p}$ is the fluid pressure and $\boldsymbol{q}$ represents sources and sinks. The porosity φ^* is given by:

$$\varphi^* = \varphi^0 + \alpha \cdot \left(\nabla \cdot \underline{u} - \varepsilon_v^0 \right) + \frac{1}{M} \left(p - p^0 \right) \tag{2}$$

where $\boldsymbol{\alpha}$ is the Biot constant, $\underline{\boldsymbol{u}}$ is the displacement vector, $\boldsymbol{\varepsilon_v^0}$ is the initial volumetric strain, M is a poroelastic constant (Gai, 2004), φ^0 and $\boldsymbol{p}^0$ account for a reference or initial state. For the mechanics part, we may start from the equilibrium equation for a quasi-steady process, which means we discard the acceleration term to come up with:

$$-\nabla \cdot \underline{\underline{\sigma}} = \underline{b} \text{ , in } \Omega \text{ ; } \Gamma = \Gamma_D^u \cup \Gamma_N^u \text{; } \underline{\boldsymbol{u}} = \underline{0} \text{, on } \Gamma_D^u \text{ ; } \underline{\boldsymbol{t}} = \underline{\underline{\sigma}} \cdot \underline{\hat{n}} \text{, on } \Gamma_N^u \tag{3}$$

where $\underline{\underline{\sigma}}$ is the stress tensor, $\underline{\boldsymbol{b}}$ is the vector of body forces, such as gravity for instance, $\underline{\hat{\boldsymbol{n}}}$ is the outer normal unitary vector. Boundary conditions (BC) usually involve prescribed tractions on part of the boundary. The mechanic problem can be decomposed in Dirichlet type BC, i.e. $\Gamma_{\boldsymbol{D}}^{\boldsymbol{u}}$, and Neumann type BC, i.e $\Gamma_{\boldsymbol{N}}^{\boldsymbol{u}}$, where the external tractions are prescribed. Hooke's law and Biot's poroelastic theory define $\underline{\underline{\sigma}}$ by:

$$\underline{\underline{\sigma}} = \underline{\underline{C}} : \underline{\underline{\varepsilon}} - \alpha \left(p - p^0 \right) \underline{\underline{\delta}} \text{ ; } \underline{\underline{C}} = \lambda \underline{\underline{\delta}} \otimes \underline{\underline{\delta}} + 2\mu \underline{\underline{\Pi}} \tag{4}$$

where $\underline{\underline{\boldsymbol{C}}}$ is the elastic moduli for isotropic elasticity, $\underline{\underline{\delta}}$ is the Kroneker delta and λ, μ are the Lamé constants, and $\underline{\underline{\Pi}}$ is the fourth-order identity tensor. The strain tensor, $\underline{\underline{\varepsilon}}$ is defined by:

$$\underline{\underline{\varepsilon}} = \nabla^s \underline{\boldsymbol{u}} = \frac{1}{2} \left[\nabla \underline{\boldsymbol{u}} + \left(\nabla \underline{\boldsymbol{u}} \right)^T \right] \tag{5}$$

by plugging Eqs. (4) and (5) into the equilibrium Eq. (3) we end up with:

$$\left(\lambda + \mu \right) \underline{\nabla} \left(\nabla \cdot \underline{\boldsymbol{u}} \right) + \mu \nabla^2 \underline{\boldsymbol{u}} - \alpha \underline{\nabla} p + \underline{b} = \underline{0} \tag{6}$$

which is the Cauchy-Navier equation of equilibrium with a formulation based on displacements. The Lamé constants can be computed in terms of familiar quantities such as Young's Modulus, E, and Poisson ratio, ν, thus:

$$\mu = G = \frac{E}{2\left(1+\nu\right)} \text{ ; } \lambda = \frac{E\nu}{\left(1+\nu\right)\left(1-2\nu\right)} \tag{7}$$

where $\boldsymbol{G}$ is the Shear Modulus.

Discretization with FEM

By plugging Eq. (2) into Eq. (1) and multiplying by a test function $\boldsymbol{v}$ and integrating over the domain yields:

$$\int_\Omega \left[\frac{1}{M} \frac{\partial p}{\partial t} + \alpha \nabla \cdot \underline{\dot{u}} - \nabla \cdot \left(\frac{1}{\mu} \underline{\underline{\boldsymbol{K}}} \left(\nabla p - \rho g \nabla z \right) \right) - q \right] \cdot v d\Omega = 0 \tag{8}$$

now, integrating by parts the term which involves Darcy's law and applying the Gauss-divergence theorem we have our weak form:

$$\int_\Omega \left(\frac{1}{M}\frac{\partial p}{\partial t} v + \alpha v \nabla \cdot \underline{\dot{u}} + \frac{1}{\mu} \underline{\underline{K}} \cdot \nabla p \left(\nabla v\right)^T \right) \cdot d\Omega = \int_\Omega q \cdot v d\Omega + \int_\Omega \left(\frac{\rho g}{\mu} \underline{\underline{K}} \cdot \nabla z \left(\nabla v\right)^T \right) d\Omega + \int_{\partial\Omega_N^p} v \frac{1}{\mu} \underline{\underline{\boldsymbol{K}}} \left(\nabla p - \rho g \nabla z\right) \cdot \underline{\hat{n}}^T ds \tag{9}$$

A weak form for the equilibrium Eq. (3) can be derived in a similar way, by testing against a given virtual displacement, thus:

$$\int_\Omega \left(\nabla \cdot \underline{\underline{\sigma}} + \underline{b}\right)^T \cdot \underline{\eta} d\Omega = 0 \tag{10}$$

after integrating by parts, using the divergence theorem as before and transposing the whole equation we indeed with:

$$\int_\Omega \left(\nabla \underline{\eta}\right)^T : \underline{\underline{\sigma}} d\Omega = \int_{\partial\Omega_N^u} \underline{\eta}^T \cdot \underline{t} ds + \int_\Omega \underline{\eta}^T \cdot \underline{b} d\Omega \tag{11}$$

where $\underline{\boldsymbol{t}} = \underline{\sigma} \cdot \underline{\hat{\boldsymbol{n}}}$ are the tractions applied as Neumman BC's. This is the well-known virtual work statement. Let us represent our primary variables in a given element $\boldsymbol{e}$, i.e. pressure and displacements, as nodal values multiplied by shape or interpolation functions:

$$\boldsymbol{p}_{\boldsymbol{e}}^{\boldsymbol{h}}\left(\underline{x}\right) = \underline{\Pi}^T \cdot \underline{\boldsymbol{p}}^{\boldsymbol{e}} \;\; ; \;\; \underline{\boldsymbol{u}}_{\boldsymbol{e}}^{\boldsymbol{h}}\left(\underline{x}\right) = \underline{\underline{\Psi}} \cdot \underline{\boldsymbol{u}}^{\boldsymbol{e}} \tag{12}$$

where $\underline{\Pi}$ and $\underline{\underline{\Psi}}$ are matrices of shape functions given by:

$$\begin{aligned} \Pi_i &= \psi_i\left(\underline{x}\right) \\ \Psi_{ij} &= \begin{cases} \psi_k\left(\underline{x}\right) & \text{if } j = \underline{\mathrm{j}} \\ 0 \text{ otherwise} \end{cases} \\ \underline{\mathrm{j}} &= DOF \cdot \left(k-1\right) + i \;\; ; \;\; k = 1 \ldots nn \end{aligned} \tag{13}$$

here $\boldsymbol{nn}$ is the number of nodes in the given element and $\boldsymbol{DOF}$ is the number of degrees of freedom which equals the space dimension (i.e. 2 for 2-D and 3 for 3-D problems). Also $\underline{\boldsymbol{p}}^{\boldsymbol{e}}$ and $\underline{\boldsymbol{u}}^{\boldsymbol{e}}$ are column vectors with nodal values of the primary variables. The displacements are stored intercalated in *(x, y, z)* chunks as shown in Eq. (14). For example these matrices are given below for a linear quadrilateral element:

$$\begin{aligned} \underline{\Pi}^T &= \begin{pmatrix} \psi_1 & \psi_2 & \psi_3 & \psi_4 \end{pmatrix} \;\; ; \;\; \underline{\underline{\Psi}} = \begin{bmatrix} \psi_1 & 0 & \psi_2 & 0 & \psi_3 & 0 & \psi_4 & 0 \\ 0 & \psi_1 & 0 & \psi_2 & 0 & \psi_3 & 0 & \psi_4 \end{bmatrix} \\ \underline{\boldsymbol{p}}^{\boldsymbol{e}} &= \begin{pmatrix} p_1 & p_2 & p_3 & p_4 \end{pmatrix}^T \;\; ; \;\; \underline{\boldsymbol{u}}^{\boldsymbol{e}} = \begin{pmatrix} u_x^{(1)} & u_y^{(1)} & u_x^{(2)} & u_y^{(2)} & u_x^{(3)} & u_y^{(3)} & u_x^{(4)} & u_y^{(4)} \end{pmatrix}^T \end{aligned} \tag{14}$$

recalling that divergence operator can be written as well as:

$$\nabla \cdot \underline{\underline{\sigma}} = \underline{\underline{D}}^T \underline{\hat{\sigma}} \tag{15}$$

since $\underline{\underline{\sigma}}$ is a symmetric tensor is convenient to represent it by a column vector $\underline{\hat{\sigma}}$ which has six independent components in 3-D or three in 2-D. The $\underline{\underline{\boldsymbol{D}}}$ operator is defined by:

$$\underline{\underline{D}}_{(2)}^T = \begin{bmatrix} \partial_x & 0 & \partial_y \\ 0 & \partial_y & \partial_x \end{bmatrix} \;\; ; \;\; \underline{\underline{D}}_{(3)}^T = \begin{bmatrix} \partial_x & 0 & 0 & \partial_y & \partial_z & 0 \\ 0 & \partial_y & 0 & \partial_x & 0 & \partial_z \\ 0 & 0 & \partial_z & 0 & \partial_x & \partial_y \end{bmatrix} \tag{16}$$

For 2- and 3-D, respectively. Now the engineering strain $\underline{\hat{\varepsilon}}$ can be defined by:

$$\underline{\hat{\varepsilon}} = \underline{\underline{B}} \underline{u}^e \;\; ; \;\; \underline{\underline{B}} = \underline{\underline{D}} \underline{\underline{\Psi}} \tag{17}$$

to wrap up the virtual work statement Eq. (11) we shall replace $\underline{\eta}$ by $\underline{\underline{\Psi}}$ which leads to:

$$\int_\Omega \underline{\underline{B}}^T : \underline{\underline{\sigma}} d\Omega = \int_{\partial\Omega_N^u} \underline{\underline{\Psi}}^T \cdot \underline{t} ds + \int_\Omega \underline{\underline{\Psi}}^T \cdot \underline{b} d\Omega \tag{18}$$

It is useful to consider the above equation as the equilibrium between internal and external forces, thus:

$$\begin{aligned}
&\underline{f}^{\text{int}}\left(\underline{u}\right)-\underline{f}^{ext}=\underline{0}\\
&\underline{f}^{\text{int}}\left(\underline{u}\right)=\int_{\Omega}\underline{\underline{B}}^{T}:\underline{\underline{\sigma}}d\Omega\ \ ;\ \ \underline{f}^{ext}=\int_{\partial\Omega_N^u}\underline{\underline{\Psi}}^{T}\cdot\underline{t}ds+\int_{\Omega}\underline{\underline{\Psi}}^{T}\cdot\underline{b}d\Omega
\end{aligned}\tag{19}$$

this equation holds for both elasticity and plasticity. Finally by plugging the generalized Hooke's law Eq. (4) into Eq. (18) and using Eq. (9) leads to our Finite Element model for isotropic poroelasticity, thus:

$$\begin{bmatrix}0 & 0\\ \underline{\underline{\mathrm{Q}}}^{T} & \underline{\underline{\mathrm{S}}}\end{bmatrix}\frac{d}{dt}\begin{Bmatrix}\underline{\boldsymbol{u}}\\ \underline{\boldsymbol{p}}\end{Bmatrix}+\begin{bmatrix}\underline{\underline{\mathrm{K}}} & -\underline{\underline{\mathrm{Q}}}\\ 0 & \underline{\underline{\mathrm{H}}}\end{bmatrix}\begin{Bmatrix}\underline{\boldsymbol{u}}\\ \underline{\boldsymbol{p}}\end{Bmatrix}=\begin{Bmatrix}\underline{\boldsymbol{f}_u}\\ \underline{\boldsymbol{f}_p}\end{Bmatrix}\tag{20}$$

where the matrixes are given by:

$$\begin{aligned}
&\underline{\underline{\mathrm{S}}}=\int_{\Omega}\frac{1}{M}\underline{\Pi}\cdot\underline{\Pi}^{T}d\Omega\ \ ;\ \ \underline{\underline{\mathrm{Q}}}=\int_{\Omega}\underline{\underline{B}}^{T}\alpha\underline{\boldsymbol{m}}\ \underline{\Pi}d\Omega\ \ ;\ \ \underline{\boldsymbol{m}}_{(2)}=\left(1,1,0\right)^{T}\ \ ;\ \ \underline{\boldsymbol{m}}_{(3)}=\left(1,1,1,0,0,0\right)^{T}\\
&\underline{\underline{\mathrm{K}}}=\int_{\Omega}\underline{\underline{B}}^{T}\underline{\underline{C}}\ \underline{\underline{B}}d\Omega\ \ ;\ \ \underline{\boldsymbol{f}_u}=\int_{\partial\Omega_N^u}\underline{\boldsymbol{t}}\cdot\underline{\underline{\Psi}}^{T}\ ds+\int_{\Omega}\underline{\underline{\Psi}}^{T}\underline{b}\cdot d\Omega\\
&\underline{\underline{\mathrm{H}}}=\int_{\Omega}\frac{1}{\mu}\underline{\underline{\boldsymbol{K}}}\nabla\underline{\Pi}\cdot\left(\nabla\underline{\Pi}\right)^{T}d\Omega\ \ ;\ \ \underline{\boldsymbol{f}_p}=\int_{\partial\Omega_N^p}\left(\frac{1}{\mu}\underline{\underline{\boldsymbol{K}}}\nabla p\cdot\underline{\boldsymbol{n}}\right)\cdot\underline{\psi}_p\ ds+\int_{\Omega}\underline{\psi}_p f\cdot d
\end{aligned}\tag{21}$$

The so called fully coupled method arises when Eq. (20) is discretized in time and so that the updates for pressures, p, and displacements, $\mathbf{u}$, are updated simultaneously, we obtain the following (Ferronato et al., 2010):

$$\begin{aligned}
&\begin{bmatrix}\underline{\underline{\mathrm{K}}} & -\underline{\underline{\mathrm{Q}}}\\ \underline{\underline{\mathrm{Q}}}^{T} & \underline{\underline{\mathrm{S}}}'\end{bmatrix}\begin{Bmatrix}\underline{\boldsymbol{u}}\\ \underline{\boldsymbol{p}}\end{Bmatrix}^{n+1}=\begin{bmatrix}\Phi\underline{\underline{\mathrm{K}}} & -\Phi\underline{\underline{\mathrm{Q}}}\\ \underline{\underline{\mathrm{Q}}}^{T} & \underline{\underline{\mathrm{S}}}''\end{bmatrix}\begin{Bmatrix}\underline{\boldsymbol{u}}\\ \underline{\boldsymbol{p}}\end{Bmatrix}^{n}+\begin{Bmatrix}\underline{\boldsymbol{f}_u}/\theta\\ \underline{\boldsymbol{f}_p}\cdot\Delta t\end{Bmatrix}\\
&\underline{\underline{\mathrm{S}}}'=\underline{\underline{\mathrm{S}}}+\theta\cdot\Delta t\cdot\underline{\underline{\mathrm{H}}}\ \ ;\ \ \Phi=\left(\left(\theta-1\right)\right)/\theta\\
&\underline{\underline{\mathrm{S}}}''=\underline{\underline{\mathrm{S}}}-\left(1-\theta\right)\cdot\Delta t\cdot\underline{\underline{\mathrm{H}}}.
\end{aligned}\tag{22}$$

In Eq. (22), q is the implicitness parameter which liea between 0 and 1.

The loose coupling approach can be obtained in different ways. One possibility is shown in Eq. (23), where the displacements are solved first taking the pressures from the previous time step. Next, pressures are updated using the new displacements:

$$\begin{aligned}
&\underline{\underline{\mathrm{K}}}\underline{\boldsymbol{u}}^{n+1}=f_u+\underline{\underline{\mathrm{Q}}}\left(p^{n}-p^{0}\right)\\
&\underline{\underline{\mathrm{S}}}'\underline{\boldsymbol{p}}^{n+1}=\underline{\underline{\mathrm{S}}}''\underline{\boldsymbol{p}}^{n}+\underline{\boldsymbol{f}_p}\cdot\Delta t-\underline{\underline{\mathrm{Q}}}^{T}\left(\underline{\boldsymbol{u}}^{n+1}-\underline{\boldsymbol{u}}^{n}\right)
\end{aligned}\tag{23}$$

An iterative coupling scheme can be defined in several different ways, but basically they draw from the loose coupling scheme with the addition of an internal iteration in order to update lagged quantities. For more details refer to (Dean et al., 2006; Gai, 2004; Kim et al., 2009). In particular, Kim et al. discussed in detail several iteratively-coupled methods for the solution of coupled flow and reservoir geomechanics for single-phase flow. They analyzed four different operator-splitting strategies that involve solving the mechanical or the flow problem first and they also included some results dealing with poro-plasticity.

Domain Decomposition Schemes

All domain decomposition methods considered here lie within the general approach of the so-called interface problems, associated with the Steklov-Poincaré operator, equivalent to the Schur complement method which is a discrete version of the interface operator. There is broad literature covering these schemes, we just attempt to do a simple introduction for the sake of completeness. The Dirichlet-Neumann (DN) DDM was considered, for example, by Bjørstad and Widlund (Bjorstad and Widlund, 1986), Bramble et al. and Marini and Quarteroni (Funaro et al., 1988) among other authors (Quarteroni and Valli, 1999).

To describe the DN-DDM, we consider an abstract differential operator $\boldsymbol{L}$, which might be the Laplace operator. The scheme consists in solving a series of problems in the right sequence, which requires a coloring tool (see Fig. 1). Let us color the Dirichlet subdomains in white and the Neumman subdomains in black. Notice also that the interface between subdomains is Γ. After providing an initial guess on the primaries variables on Γ, i.e., λ^{k} must be given, we may solve the problem on the white subdomains (Dirichlet problems) which is the step 1 on Eq. (24).

Let us call the primary variable "displacements", and "tractions" their gradient or normal derivative in the boundary. After solving step 1 on the white subdomains we compute the tractions on the interface Γ which can be pass to solve step 2 on the black subdomains, i.e. Neumann subdomains. On these latter ones, since the tractions are being passed on Γ we can solve for unknown displacements which provide feedback for the next iteration level.

$$1)\begin{cases} Lu_1 = f \ \text{ in } \ \Omega_1 \\ u_1{}^{k+1} = 0 \ \text{ on } \ \partial\Omega_1 \cap \partial\Omega \\ u_1{}^{k+1} = \lambda^k \ \text{ on } \Gamma \end{cases} \qquad 2)\begin{cases} Lu_2 = f \ \text{ in } \ \Omega_2 \\ u_2{}^{k+1} = 0 \ \text{ on } \ \partial\Omega_2 \cap \partial\Omega \\ \partial_n u_2{}^{k+1} = \mu^{k+1} \ \text{ on } \Gamma \end{cases} \tag{24}$$

To improve the convergence both displacements and tractions must be overrelaxed, the relaxation parameters θ^D and θ^N lie between 0 and 1 as shown in Eqs. (25):

$$\begin{aligned} \lambda^{k+1} &= \left(\theta^D \cdot u_2{}^{k+1} + \left(1-\theta^D\right)\cdot u_1{}^k\right)_\Gamma \\ \partial_n u_2{}^{k+1} &= \left(\theta^N \cdot \partial_n u_1{}^{k+1} + \left(1-\theta^N\right)\cdot \partial_n u_2{}^k\right)_\Gamma \end{aligned} \tag{25}$$

It turns out that this scheme may require a three-entry coloring tool because for general partitioning some subdomains may become hybrid as they are in contact with both Dirichlet and Neumann neighbors. There is a lack of parallelism in the sense that the black subdomains must wait for the others to communicate tractions. This problem can be mitigated by prescribing tractions as initial guess, but this is not straightforward in most cases. An easy way to provide an initial guess for the multiplier λ^k is by doing a so-called coarse-run, which means solving the same problem in a coarser mesh and assigning λ^k on Γ by standard interpolation, using the finite element space from the coarse problem. In our code, we have the ability to provide an initial guess. For proof of convergence and further details about this scheme we refer the reader to the literature (Quarteroni and Valli, 1999; Toselli and Widlund, 2004).

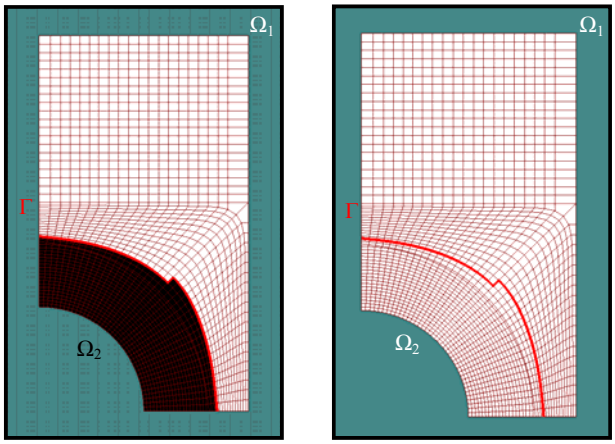

Figure 1: Domain Decomposition schemes. The Dirichlet-Neumann (left) and the Neumann-Neumann (right) schemes are depicted.

The Neumann-Neumann (NN) DDM was presented by Bourgat et al. (Bourgat et al., 1988), a previous version was investigated by Agoshkov and Levedev (Quarteroni and Valli, 1999). The Balancing Domain Decomposition (BDD) was introduced by Mandel by adding a coarse problem to the Neumann-Neumann method, which is closely related with the method of Glowinski and Wheeler for mixed problems (Glowinski and Wheeler, 1988). The development of BDD was motivated by the good performance of the Neumann-Neumann preconditioner for real-wold problems with strongly discontinuous coefficients for a small number of subdomains (Cowsar et al., 1995). The NN-DDM does not require a coloring tool, indeed each subdomain is of Dirichlet type, after providing λ^k we can solve them completely in parallel as shown in the first step on Eq. (26):

$$\begin{aligned} &1)\begin{cases} Lu_i = f \ \text{ in } \ \Omega_i \\ u_i{}^{k+1} = 0 \ \text{ on } \ \partial\Omega_i \cap \partial\Omega \\ u_i{}^{k+1} = \lambda^k \ \text{ on } \Gamma \end{cases} \qquad 2)\begin{cases} L\psi_i = 0 \ \text{ in } \ \Omega_i \\ \psi_i{}^{k+1} = 0 \ \text{ on } \ \partial\Omega_i \cap \partial\Omega \\ \partial_n \psi_i{}^{k+1} = \partial_n u_1{}^{k+1} + \partial_n u_2{}^{k+1} \ \text{ on } \Gamma \end{cases} \\ &\lambda^{k+1} = \lambda^k - \theta\cdot\left(\sigma_1\cdot\psi_1{}^{k+1} - \sigma_2\cdot\psi_2{}^{k+1}\right)_\Gamma . \end{aligned} \tag{26}$$

The second step on Eq. (26) corresponds to the Neumann step, which is the preconditioner for this scheme, to do so we may

get the residual in tractions on the subdomain interfaces by communication. It turns out that this traction residual is going to be the driving force for this problem. After solving the Neumann step we may feedback λ^k by using a recursive relationship in Eq. (26). The parameter θ is usually set to 0.5, whilst ψ_1, ψ_2 are integer tuning constants usually set to 1 (Quarteroni and Valli, 1999) .

When this scheme converges, it does so faster than the Dirichlet-Neumann scheme. In terms of communication the NN-DDM requires twice the communication cost of Dirichlet-Neumann per iteration, notices that setting up step 2 requires a first communication and to feedback λ^k a second communication round is required. The scheme also requires two solves per iteration, the Dirichlet step can be seen as the action of the interface operator because accounts for λ^k while the Neumann step plays the role of preconditioner.

The NN-DDM scheme is attractive due to its first completely parallel step and also by incorporating a good preconditioner. For general partitions, each subdomain's Dirichlet and Neumann problems are well-posed if all subdomains touch the global boundary. In some cases internal subdomains may not be in contact with the global boundary, those subdomains shall require a special treatment in order to remove rigid body motions, i.e. to guarantee existence and uniqueness of these local problems. A fairly general implementation will require a BDM approach, which uses a coarse-problem to control those subdomains problems and to ensure that a global error exchange takes places among subdomains, see (Mandel and Brezina, 1996) for details and also a conjugate gradient iteration to feedback displacements with the Neumann step as preconditioner.

Mortar Finite Element methods (MFEM) were introduced by Bernardi, Maday and Patera for the Poisson equation in (Bernardi et al., 1994b) in order to formulate a weak continuity condition at the interface of subdomains in which different variational approximations are used. Relaxing the constraint on the boundaries of the interfaces, the formulation of Belgacem (Belgacem, 1999) with Lagrange multipliers is the standard framework in which the method is understood at present time. One of the key aspects of the method consists of defining appropriate spaces of Lagrange multipliers for enforcing the gluing constraint (Hauret and Ortiz, 2006). Additional references dealing with Mortars methods can be found but are not limited to (Babuska, 1973; Flemisch et al., 2005; Hansbo et al., 2005; Kim et al., 2001; Kim et al., 2005; Lamichhane et al., 2005; Maday et al., 1988; Wohlmuth, 2000). The reader may also refer to (Destuynder and Roux, 1988; Flemisch et al., 2005; Hansbo et al., 2005; Hauret and Le Tallec, 2007; Puso, 2004) for specific applications to isotropic elasticity and elliptic problems.

Let us describe MFEM for linear isotropic elasticity in terms of bilinear forms, $\boldsymbol{a}$, β defined in Eq. (27) below,

$$\begin{aligned} a\left(\underline{\boldsymbol{u}},\underline{\boldsymbol{v}}\right) &= \int_{\Omega} \underline{\varepsilon}\left(\underline{\boldsymbol{v}}\right)^T \cdot \underline{\underline{C}} \cdot \underline{\varepsilon}\left(\underline{\boldsymbol{u}}\right) d\Omega \;\; ; \;\; l\left(\underline{\boldsymbol{v}}\right) = \int_{\partial\Omega^N} \underline{\boldsymbol{t}} \cdot \underline{\boldsymbol{v}} \; ds + \int_{\Omega} \underline{b} \cdot \underline{\boldsymbol{v}} \; d\Omega \\ \beta\left(\underline{\boldsymbol{u}},\underline{\boldsymbol{v}}\right) &= \int_{\Gamma} \left[\underline{\boldsymbol{u}}\right] \cdot \underline{\boldsymbol{v}} \; d\Gamma \;\; ; \;\; \left[\underline{\boldsymbol{u}}\right] = \left(\underline{\boldsymbol{u}}^{(1)} - \underline{\boldsymbol{u}}^{(2)}\right), \end{aligned} \tag{27}$$

where β stands for gluing condition among subdomain interfaces, we require that the jump $\left[\underline{\boldsymbol{u}}\right]$ on the displacements to vanish in an integral or "weak" sense, thus:

$$\begin{cases} a\left(\underline{\boldsymbol{u}}_h,\underline{\boldsymbol{v}}_h\right) + \beta\left(\underline{\boldsymbol{v}}_h,\underline{\lambda}_h\right) = l\left(\underline{\boldsymbol{v}}_h\right) \\ \beta\left(\underline{\boldsymbol{u}}_h,\underline{\mu}_h\right) = 0 \end{cases} \tag{28}$$

in Eq. (28) $\underline{\mu}_h$ is the mortar space. In algebraic or matrix form, Eq. (28) can be written as:

$$\begin{bmatrix} \left[k^{(1)}\right] & [0] & \left[\beta^{(1)}\right]^T \\ [0] & \left[k^{(2)}\right] & -\left[\beta^{(2)}\right]^T \\ \left[\beta^{(1)}\right] & -\left[\beta^{(2)}\right] & [0] \end{bmatrix} \cdot \begin{bmatrix} \underline{\boldsymbol{u}}^{(1)} \\ \underline{\boldsymbol{u}}^{(2)} \\ \underline{\boldsymbol{\lambda}} \end{bmatrix} = \begin{bmatrix} \underline{\boldsymbol{l}}^{(1)} \\ \underline{\boldsymbol{l}}^{(2)} \\ \underline{\boldsymbol{0}} \end{bmatrix} \tag{29}$$

This is the so-called saddle-point problem. Notice that subdomains are only connected by means of the Lagrange multiplier $\underline{\boldsymbol{\lambda}}$, if one knows this it is possible to decouple the system in Eq. (29) and then just perform subdomain solves. The rectangular matrices $\left[\beta^{(i)}\right]$, $\boldsymbol{i} = 1 \ldots 2$, are called projectors since they allow to map to and from the mortar space. To compute the projector, special quadrature rules must be employed:

$$\beta_{ij}^{(k)} = \int_{\Gamma} \varphi_j^{(k)} \, \mu_i \, ds \tag{30}$$

where $\varphi_j^{(k)}$ represents the global non-mortar side interpolation functions and μ_i are the mortar space basis function. The integration must be carried out on subdomain interfaces always in a parametric or computational space; two-dimensional problems will involve 1-D integrals among curves while three-dimensional problem will require integrals over surfaces. Generally speaking the mortar projector can be seen as L^2 projector which allows projecting onto the mortar space by using $[\beta]$ and its transpose to map to a non-mortar side. Several DDM are available to decouple the saddle point problem Eq. (29), both DN- and NN-DDM can be applied almost without major modifications. The additional considerations to do so are the following:

1. The communication cost is a function of the dimension of the mortar space, i.e. the number of mortar degrees of freedom.
2. Non-mortar-to-Mortar and Mortar-to-Non-mortar maps must be carried out before and after performing any communication between subdomains. Subdomain's data structures must include the projector and its transpose to perform these mappings efficiently per iteration.

These changes are quiet reasonable since the only thing in common among subdomains interfaces is the mortar space, the way to transfer information from one side to the other is by defining a common format, which is mapping to the mortar space. In a computer implementation a wrapper interface mapping to the mortar before sending any data over MPI must be implemented. After receiving any data another mapping is required. Most of the implementation overhead lies in computing the projector, the communication wrappers dealing with mapping before and after are minor modifications for a given parallel application.

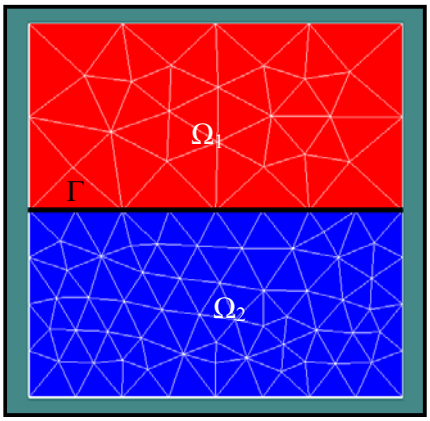

Figure 2: Non-matching interfaces and hanging-nodes are treated properly by means of the MFEM.

In recent years there have been numerous developments in applying non-overlapping domain decomposition methods for linear elasticity based upon a displacement formulation using mortar spaces (Bernardi et al., 1994a; Fritz et al., 2004; Hauret and Ortiz, 2006). All of these approaches employ Lagrange multipliers as traction boundary conditions and may require the solution of a coarse grid problem for elimination of rigid body motions if the decomposition involves more than two subdomains (Girault et al., 2009). For instance, Hauret and Ortiz (Hauret and Ortiz, 2006) discussed about the convergence of mortar methods applied to linear elasticity.

In the context of reservoir compaction and subsidence estimation it is common to deal with serial legacy codes for flow. Indeed, major reservoir simulators such as compositional codes lack parallelism. Another issue is the fact that, generally speaking, flow and mechanics domains are different. At first glance, one may consider using the same mesh for flow and mechanics, at least in the so-called pay-zone. Meshing only in the pay-zone brings the in-situ stresses into the picture as Neumann boundary conditions, which is limited due to the uncertainties to measure or compute them accurately. Another approach is to extend the reservoir mesh somehow on its surroundings (i.e. non-pay-zone), which increases the computational cost by generating a huge mesh for mechanics but it allows dealing with simpler Dirichlet boundary conditions for displacements instead. This last alternative is more tractable besides its additional computational effort.

A serial-parallel software architecture is depicted in Fig. 3. The pay-zone is shown in red while its surroundings are represented in light-blue. The mechanic domain is partitioned in two evenly pieces as shown in the bottom. The communication work-flow is flow-driven; the flow processor shall broadcast pressure drop information to those mechanic processors touching the pay-zone. Then mechanic processors can send back stresses and/or strains to the flow processor, which plays the role of dispatcher. In this paper, we will present some results involving this strategy which seems to be promising to

couple flow and mechanics on different domains. The following steps must be considered to do these changes in a given serial-flow code:

1. Create pressure-drop communication tables.
2. A mechanics type processor in contact with the pay-zone performs the following high level inner steps:
   Receive pressure drop: *Add MPI communication layer*
   Refresh RHS for accounting for new pressure-drop loading
   Solve domain decomposition problem: matching process with neighboring mechanic processors
   Send back stresses and/or strain: *Add MPI communication layer*
3. Non-pay zone processors do not get any pressure-drop information but they still need to perform inner iterations in order to match neighboring subdomains according to current DDM.

This procedure is similar to time-stepping a transient problem with DDM, the single phase flow model given by Eq. (9) is a good example. If a parallel flow code is available then a parallel-parallel coupling architecture can be developed in a similar way.

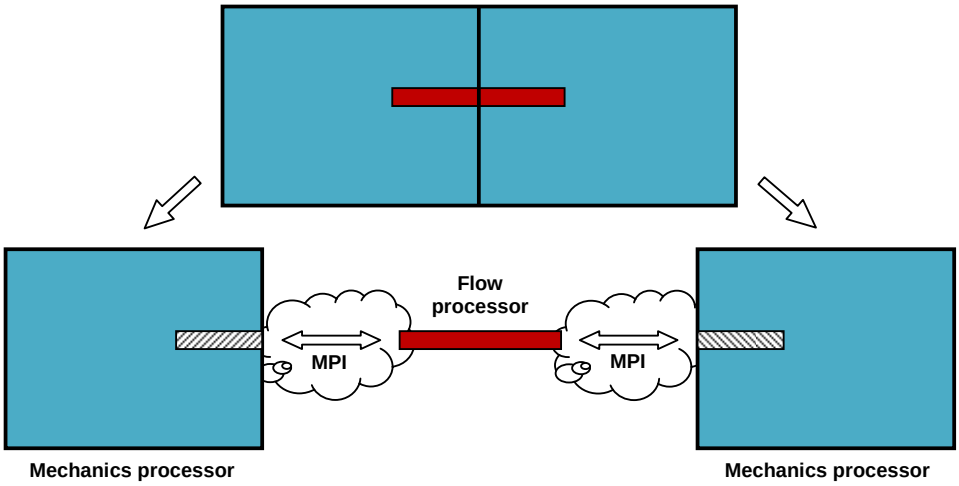

Figure 3: The serial-parallel software paradigm is graphically depicted.

Numerical Examples

In this section we present four examples, in first place a classical benchmark problem then reservoir compaction and subsidence on two- and three-dimensional synthetic cases and finally a near borehole example which is an interesting application of MFEM. We ran all these cases on a Windows desktop machine with two Intel Q9000 quad core processors at 2.00 GHz.

All numerical examples were implemented in the Integrated Parallel Finite Element Analysis program (IPFA), which is a parallel C++ application being developed at the Center for Surface Modeling at The University of Texas at Austin. IPFA's main characteristics include but are not limited to:

1. A general purpose pre- and post- processor for partitioning 2- and 3-D general structured and unstructured meshes.
2. Both serial and parallel code already validated on some benchmark problems.
3. A Python™ wrapper interface to do all FEM analysis and visualization.
4. Domain Decomposition methods for dealing with geomechanical problems and single-phase flow.

Other important aspects that have been considered in this program include pre- and post-processing, geometry and gridding. Since coupled flow/geomechanics simulations usually require complex workflows, a Python scripting interface has been developed to allow programming capabilities for preprocessing, defining geometries, gridding, post-processing and visualization. The final version of this code will be integrated with mayor reservoir simulators via loose and/or iterative coupling.

Example 1—Mandel's Problem. Mandel's problem (Mandel, 1953) is a common benchmark for coupled flow/geomechanics codes. The original work only provides a series solution for the pressure, later Abousleiman et al. (Abousleiman et al., 1996) extended that closed-form solution to include displacements and stresses. We refer the reader to the following references to look at the power series expressions (Abousleiman et al., 1996; Gai, 2004; Kim et al., 2009; Mandel, 1953; Phillips, 2005). Only a quarter of the domain needs to be simulated due to symmetry, we took the same data input used by Gai (Gai, 2004)

plus a fluid viscosity of 1E-3 Pa ·sec, which equals water dynamic viscosity at standard conditions. The domain is 100 m x 20 m and the mesh size is 44 x 66 which leads to 2904 quadrilateral elements as shown in Fig. 4. The BC for mechanics are depicted also in Fig. 3; no vertical displacement in the bottom, a traction-free right side, constant vertical stress (F / a), where $a = 10\ m$ and $F = 1E+8\ N$ (see Gai for details), symmetry on the left which implies no horizontal displacement.

The BC imposed for flow are impermeable walls on top and bottom, zero reference pressure on the right side and symmetry on the left (which leads to impermeability as well). It turns out that the driving force in this problem is the vertical stress applied on the top. This problem is equivalent to the squeezing of a 2-D sponge, which implies that the pressure must deplete until the pressure equilibrates.

Mandel's solution does not only provide one of the most popular benchmark cases for poroelasticity codes but also demonstrates a non-monotonic pressure response under constant boundary conditions (Gai, 2004; Mandel, 1953). This behavior is known as the Mandel-Cryer effect. The effect refers to the fact that besides the initial instantaneous increase, pressure at the center continues to increase for some time before it starts to drop.

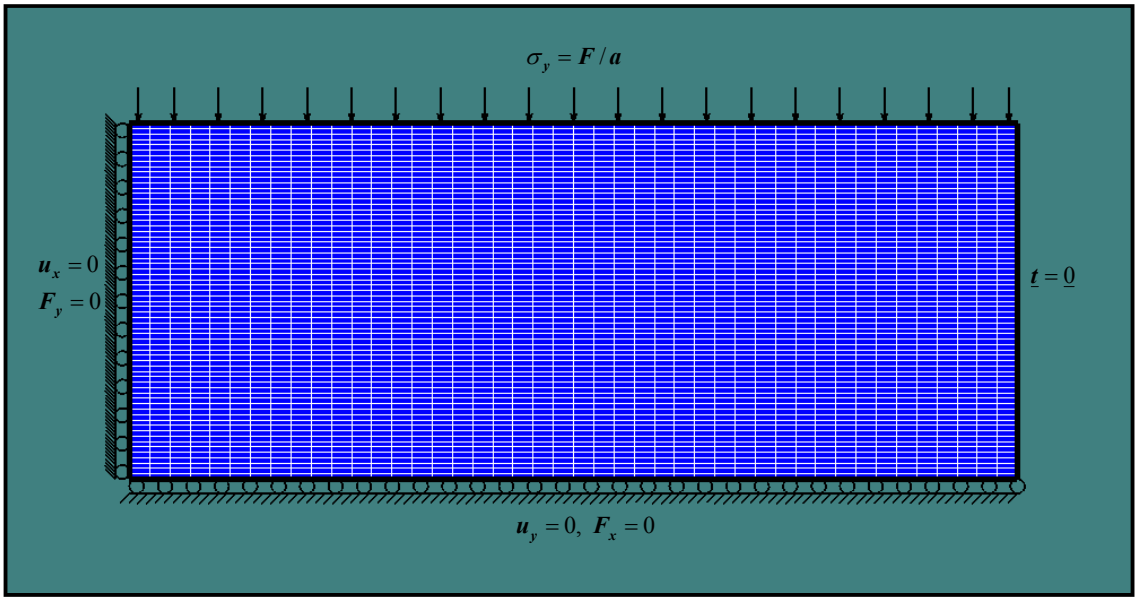

Figure 4: Mandel's problem mesh, geometry and BC's for mechanics are depicted.

Fig. 5 shows traces at $y=0$ of both dimensionless pore pressure, i.e. normalized after dividing by constant vertical stress, and horizontal displacement for different times. The curves show good agreement between the analytical (continuous lines) and numerical solution (symbols). We ran this problem by using a monolithic approach and loose coupling (a mechanic step by each pressure step) and achieved good results with both methods and in both serial and serial-serial respectively. The Mandel-Cryer effect can be clearly seen on the green curve to the left hand-side on Fig. 5. Fig. 6 depicts pressure snapshots after 1E+3 and 1E+5 secs respectively; again the overpressure area is shown in red in the color contour at the bottom.

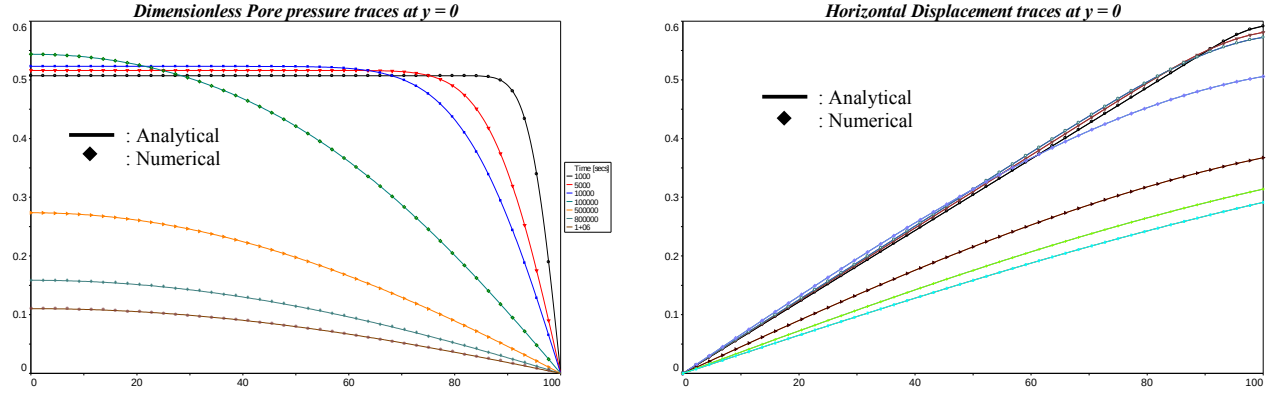

Figure 5: Dimensionless pressure and horizontal displacement traces are shown at different times.

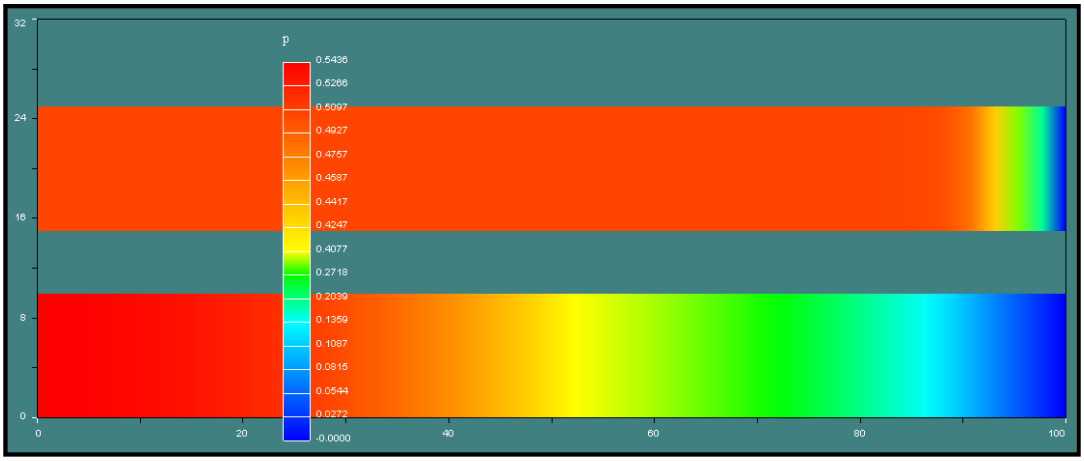

Figure 6: Dimensionless pressure snapshots are shown after 1E+3 (top) and 1E+5 (bottom) secs respectively (not to scale).

Mandel's problem raises the question about when it is really necessary to do a mechanics step per flow step. The slow evolution of the displacements suggests that a "loose coupling" strategy will lead to good results, even performing a mechanic step after several flow steps. But neither error indicator nor estimator is available to reliably tell when a mechanic step must be performed. Other interesting benchmarks for poroelasticity are the Terzaghi 1-D problem (Phillips, 2005) and its 2-D extension (plane-strain) and 3-D version (so-called squeeze of a sponge (Kaasschieter and Frijns, 2003)), also available for the same purpose.

Example 2—SPE 10 2-D layer. This example deals with reservoir compaction and subsidence in a two-dimensional conforming-mesh case. The geometry and boundary conditions for mechanics are depicted in Fig. 7. The pay-zone mesh is 100x20 quadrilaterals elements, with constant porosity and permeabilities coming from the case 1 of the SPE 10 Comparative Solution Project. The BC for flow are very simple, 1000 Psi pressure gradient between the sides and no-flow on top and bottom of the reservoir. The initial condition consists in a constant pressure, 1000 Psi in the whole flow domain. The BC for mechanics are the typical ones for these problems: traction free on the top, no horizontal displacement on the sides and no vertical displacement at the bottom, the initial displacement field is assumed to be zero. For mechanics we considered isotropic elasticity in plane-strain with mechanical properties for both the reservoir and its surroundings given by $E = 30$ ksi and $\nu = 0.3$. The reservoir length and height are 11 km and 0.3 km respectively. The over- and under-burden heights are 3 and 12 km respectively while the side's burden length is 11 km as well. The tensor-product mechanics mesh consists in 8960 elements. Fig. 7 depicts a typical mechanic's domain METIS' partition in 4 subdomains and the coloring associated to the NN-DDM. The fluid viscosity is 0.1325 cp and its Biot Modulus is 357142.85 Psi^{-1}.

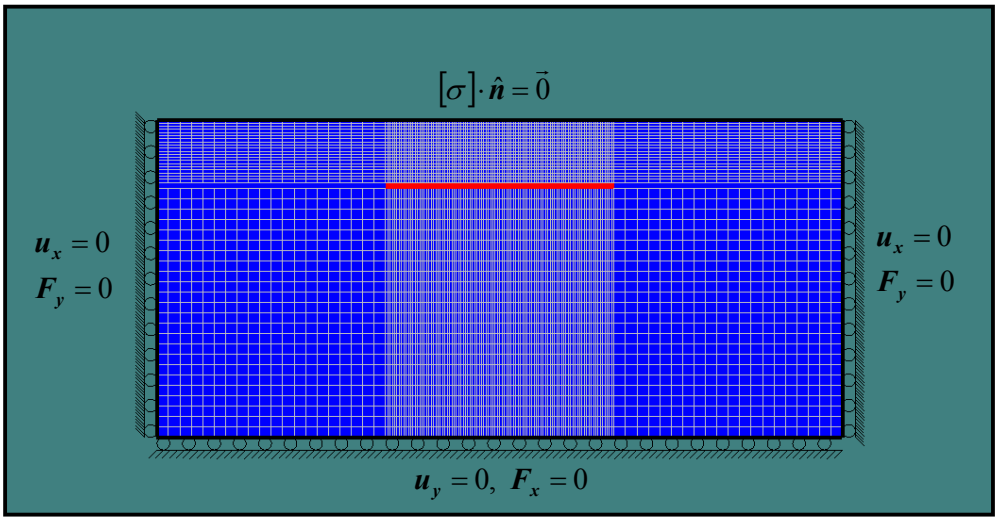

Figure 7: Synthetic reservoir compaction and subsidence two-dimensional case on plane strain is depicted.

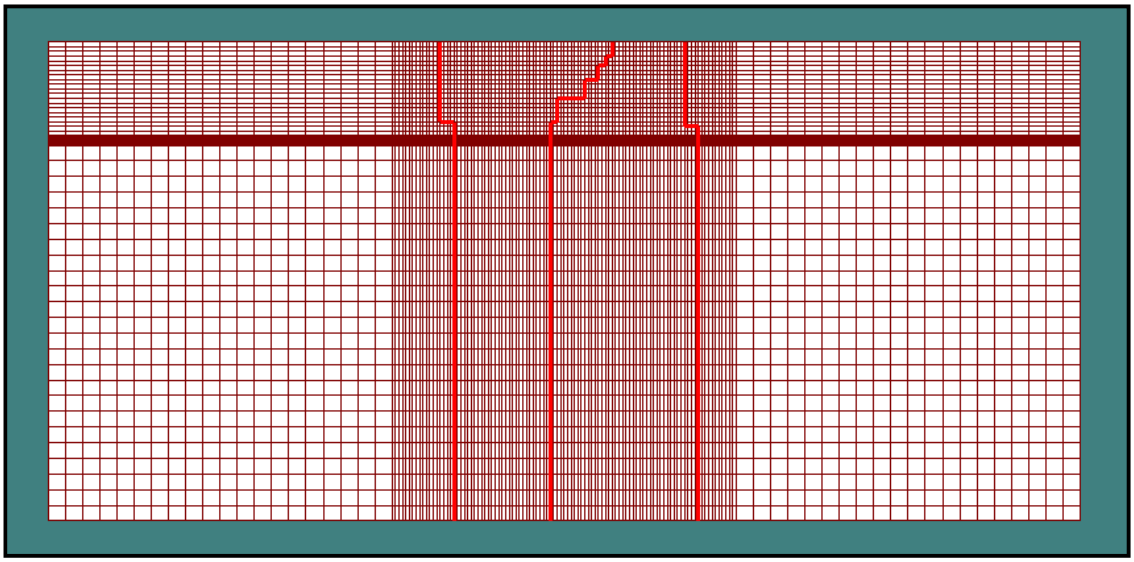

Figure 8: Partitioning in four sub-domains for NN-DDM, METIS provided a good balanced among subdomains each one with around 2.2K elements.

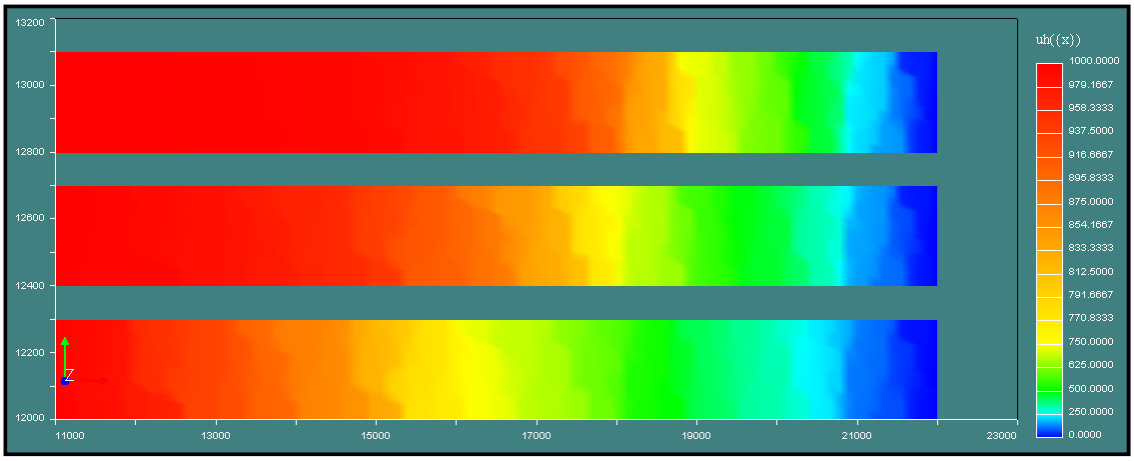

Figure 9: Snapshots show pressure field evolution, from top to bottom, after 10, 20 and 40 years of production respectively.

We employed the serial-parallel architecture describe before which allows coupling serial flow codes with a parallel mechanic codes. After 40 years of evolution the pressure reaches its steady-state solution as shown in Fig. 9 (plot not to scale). The resulting pressure drop is the driving force which induces compaction and subsidence. On Fig. 9 snapshots showing the displacement field evolution (only the area with major displacement contrast is being shown), since the pressure drop profile is not symmetric a resulting non-symmetric displacements is expected. Local deformation propagates in the vertical direction causing a subsidence of the surface (See Fig. 10, right-column). The reservoir compaction pattern shows a build-up at the bottom and compaction at the top. Fig. 11 depicts the solution to the NN-DDM preconditioner problem. The color contours shown represent the so-called "trace" of the multiplier λ^k on the subdomains. Discontinuities at the interface between the subdomains are apparent from this figure. The matching process consists of killing off that residual or difference on tractions at the interface. For this specific problem, two or three inner iterations are usually required for convergence.

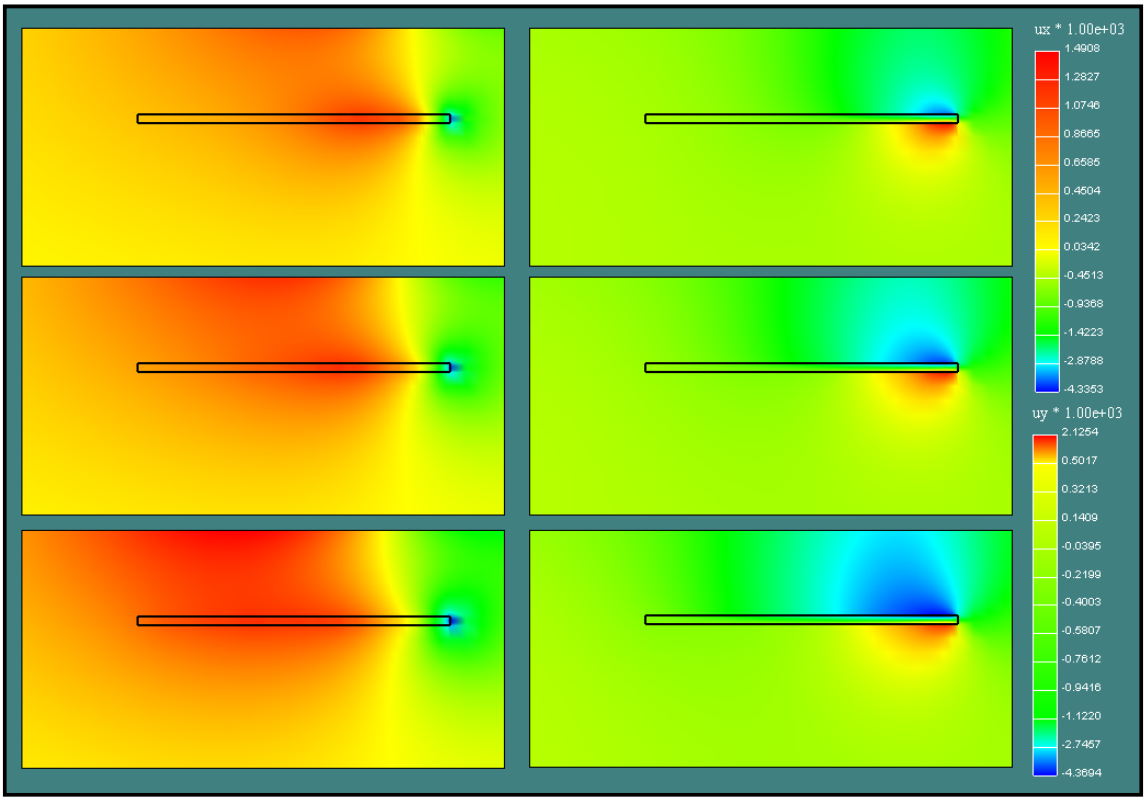

Figure 10: Snapshots show displacement field evolution, from top to bottom, after 10, 20 and 40 years of production respectively. Horizontal displacements are to the left, whilst vertical ones are to the right. The pay-zone area is highlighted in black (plot to scale).

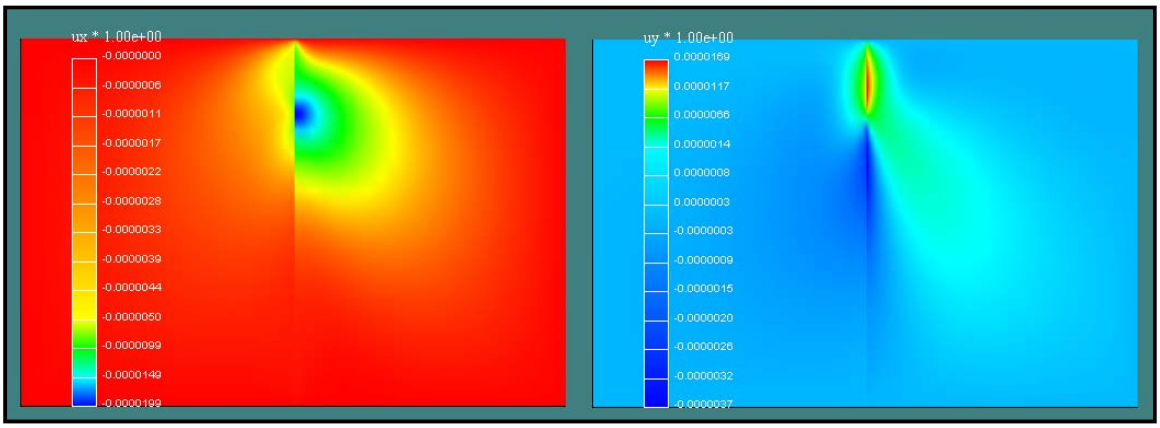

Figure 11: Solutions to the Neumann-Neumann preconditioning problem are depicted.

Example 3—Synthetic 3-D reservoir. This example corresponds to the 3-D version of the previous one. Fig. 12 depicts the geometry of the reservoir which consists in 1696 elements (23x8x9). The boundary conditions for both flow and mechanics are similar to those described already in the previous example except to include the new dimension. Fig. 13 shows a cut of the mechanic's mesh which consists in roundly 16000 hexahedral elements; the reservoir was extended into its surroundings as shown. The reservoir convex-hull dimensions are (17830, 5850, 3200) in the x-, y- and z-directions respectively. The mechanics volume convex-hull box is (60761, 48741, 15359), all dimensions are in meters here. This reservoir corresponds to a coarser version of the Brugge-field, a well known dataset for model reduction and parameter estimation, whose geometry was reconstructed by using NURBS surfaces and then extrapolated into its over-, under- and side-burdens. In this case both porosity and permeability data come from the SPE 10 Comparative Solution Project, the fluid viscosity and the mechanical properties are the same as above. Fig. 14 shows a pressure snapshot after several years of production, notice that the pressure behavior looks similar to that described in the two-dimensional case. Finally Fig. 15 depicts the vertical displacement color

contour which reproduces a similar compaction area (blue area) propagating from the reservoir to the surface, again consistent with the 2-D case.

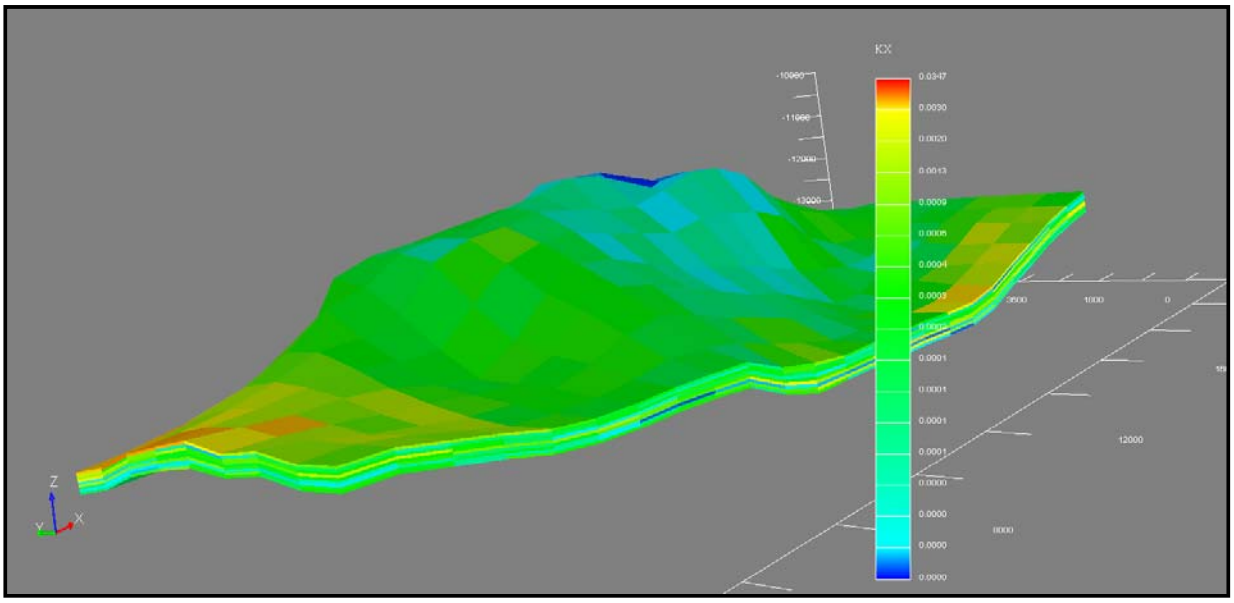

Figure 12: 3-D reservoir's geometry showing a permeability color contour is depicted (The plot is exaggerated six times in the vertical direction).

The goal of this example is to show that the serial-parallel approach extends to a 3-D realistic case in a straightforward way; we may also expect to achieve a better speedup that the obtained in the previous case. This expectation is justified by the fact that now, in a 3-D setting, to assemble the stiffness and load vector is going to take way more time compared against 2-D case. The completely parallel assembling will be an advantage in this case for sure. An updated version of this example will be presented at the conference including speedup results.

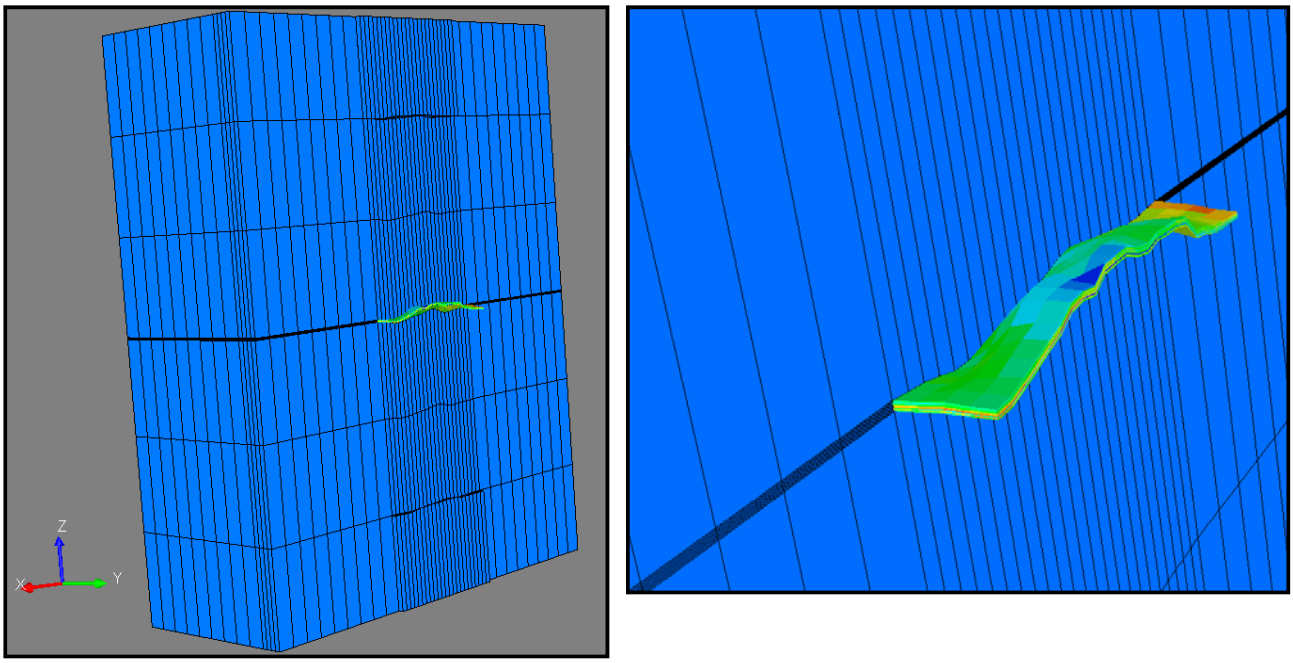

Figure 13: Half of the mechanic's mesh is depicted. The pay-zone in the center is included to provide a reference (the plot is exaggerated six times in the vertical direction).

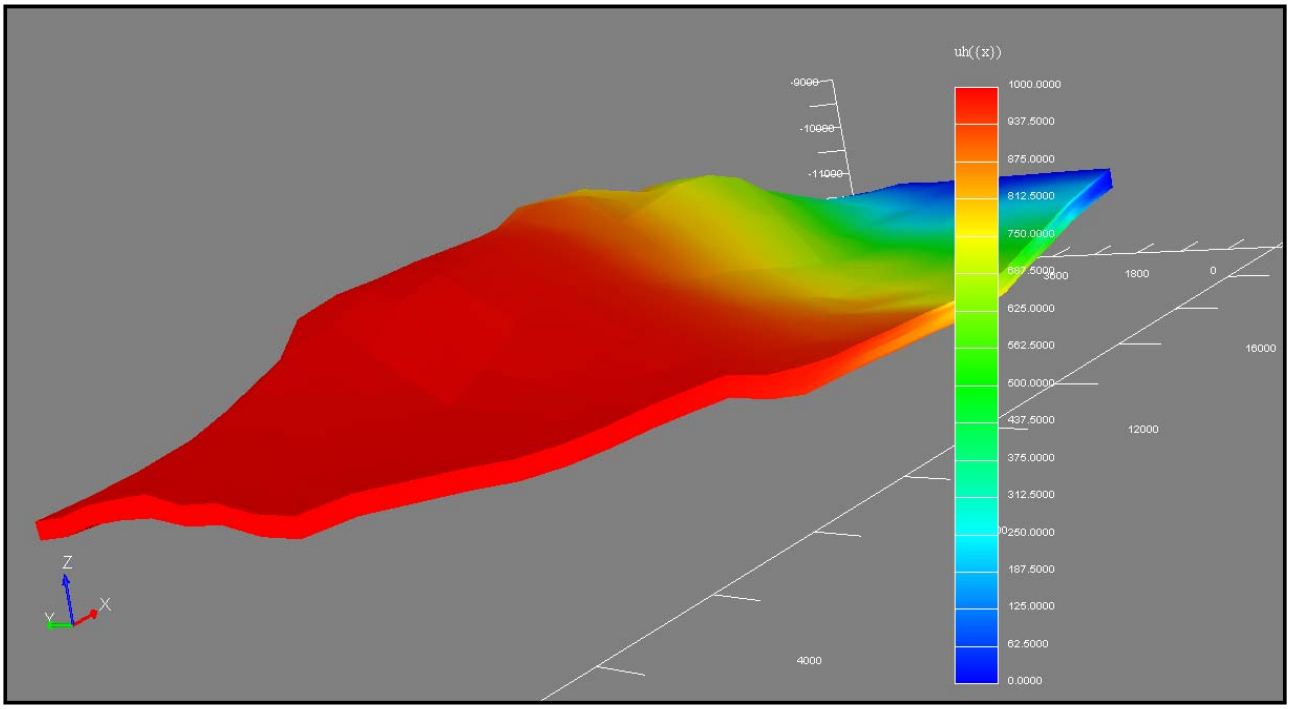

Figure 14: A pressure field snapshot is shown after several years of production.

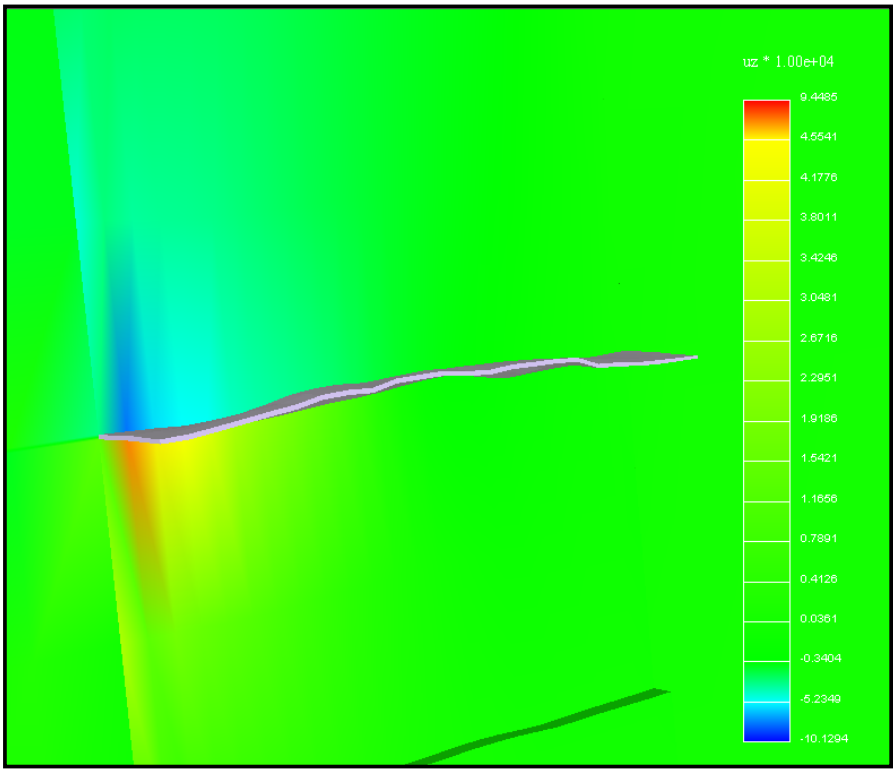

Figure 15: A snapshot shows displacement field color contour, the pay-zone area is highlighted in grey.

Example 4—Near borehole 3-D section. This example consists in a 3-D version of the well-known Bradley problem (Charlez, 1991; Fjaer et al., 2008). Bradley extended the famous Kirsch's solution, which provides the stress field in a cylindrical hole due to constant tension load at infinity (Barber, 2002), for the case where there is internal pressure in the hole, i.e. the well's

pressure or mud-weight for instance. This is a important solution being implemented in major commercial codes dealing with near-borehole geomechanics based on well-logs which allows computing allowable mud-window or borehole stability parameters, even sand production parameters as well (Belayneh, 2004; Muller et al., 2009; Santarelli et al., 1992). In the general case the stress concentration around the hole leads to the development and propagation of a plastic zone whose adequate representation requires a fine grid. In addition, different physical behaviors might occur, i.e. plasticity in the inner cylinder and elasticity in the outer part of the domain. The goal of this example is to show that the mortar approach is useful to tackle problems of this sort as it can help the merging of different subdomains by imposing adequate matching conditions.

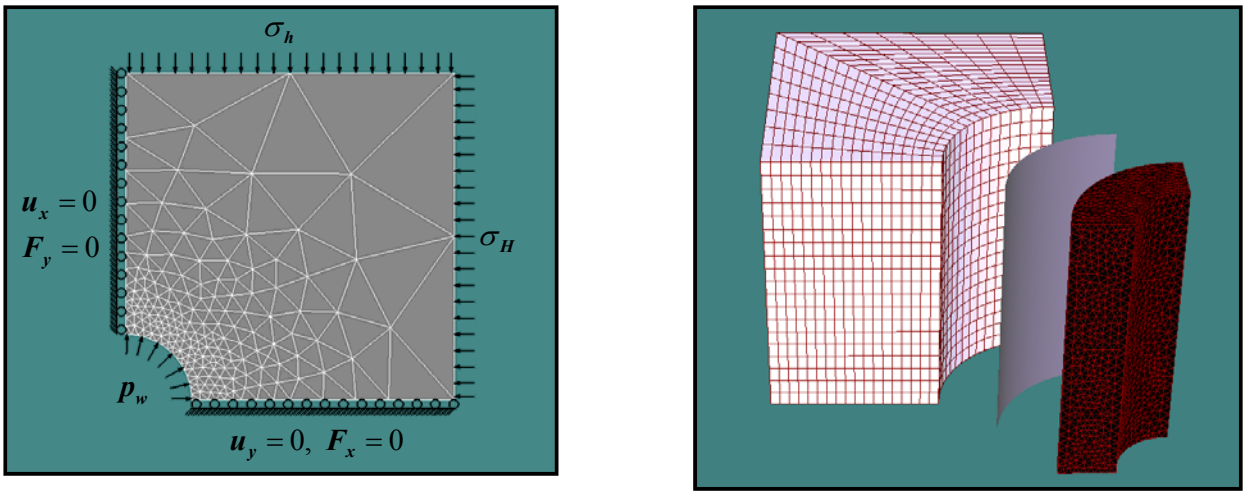

Figure 16: The geometry, BC's, and the computational meshes for Bradley's 3-D problem are depicted (to scale).

A first approach to solve this problem considers homogeneous isotropic elasticity using non-conforming meshes on different domains. Fig. 16 (left) describes the problem geometry and BC, we have the well's pore pressure in the hole, symmetry requires displacements to vanish on the bottom and left sides while the in-situ stresses prescribed in the remaining (horizontal) sides, as shown in the figure. In the z-direction (perpendicular to the paper) we have no displacement in the bottom and a traction-free surface on the top. We use the DN-DDM to decouple the saddle-point problem, thus the coloring, the mortar surface in grey and the meshes for each domain are being shown in Figure 16 (right). The Dirichlet hexahedral subdomain (in white) contains 2736 elements whilst the tetrahedral Neumann mesh (in black) consists in 20836 elements respectively. The hole's radius is 5 inches, which is a typical caliper value for a well, and the cube side is 25 inches.

The mechanical properties and values for boundary conditions are shown in Eq. (31) below,

$$\begin{aligned} & p_w = 50 \\ & \sigma_H = 80, \quad \sigma_h = 20 \\ & E = 5 \cdot 10^3, \quad \upsilon = 0.25 \\ & [\mathrm{P}] = \mathrm{MPa} \\ & \sigma = \left(\sigma_H + \sigma_h\right)/2.0 = 50 \\ & \left(x\right)^* = \left(x/\sigma\right) \ ; \ p_w^* = 1.0 \end{aligned} \tag{31}$$

where we normalize stress parameters by dividing by the average in-situ stress, al stress and pressure units are in MPa.

In order to compute the projector's entries, surface integrals in Eq. (30) must be evaluated. To do so, special quadrature rules can be developed in the computational space. Figure 17 depicts the mortar surface and shows a mortar mesh in red and a non-mortar mesh in white. In this example, the mortar space consists of 16 piecewise linear quadrilateral elements, for the sake of simplicity, it is better to do quadrature on the non-mortar mesh, i.e. in the triangular mesh in this case. When computing a given triangle contribution, one needs to know what are the mortar quads being touched by this triangle, since the shape functions have local support, all functions must be clipped out or confine to their elements, which implies any evaluation outside must return zero. In order to efficiently perform these intersections among elements, we choose our mortar mesh to be a tensor product rectangular mesh. Then, a very efficient “range-search” algorithm can be used: quad-trees for instance provide an answer to this requirement. Most of the computational cost to compute the projector lies on intersecting elements.

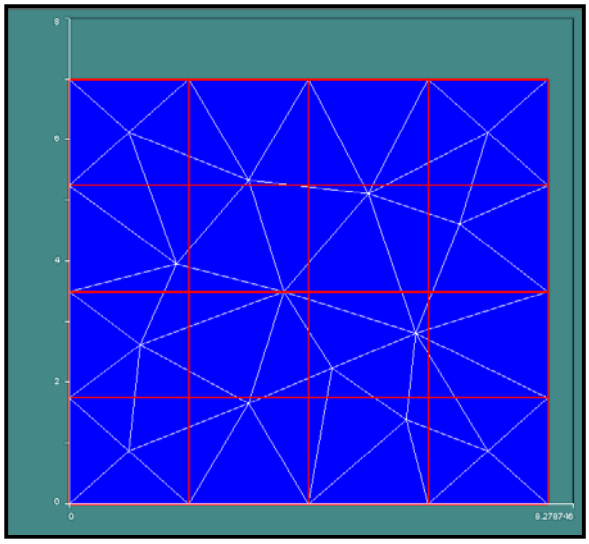

Figure 17: A special quadrature rule on parametric space must be implemented.

The projector's action is depicted in Fig. 18 where the Neumann's subdomain sends its displacement to feedback the next Dirichlet step (from left to right in the figure). We can see that the projector is an interpolant, allowing these non-matching sides to communicate with each other. The interpolation is defined in integral or weak sense; this also gives the method a multi-scale flavor. Indeed, the mortar method can be seen as a variational multi-scale finite element method (Destuynder and Roux, 1988; Flemisch et al., 2005; Hansbo et al., 2005; Hauret and Le Tallec, 2007; Puso, 2004).

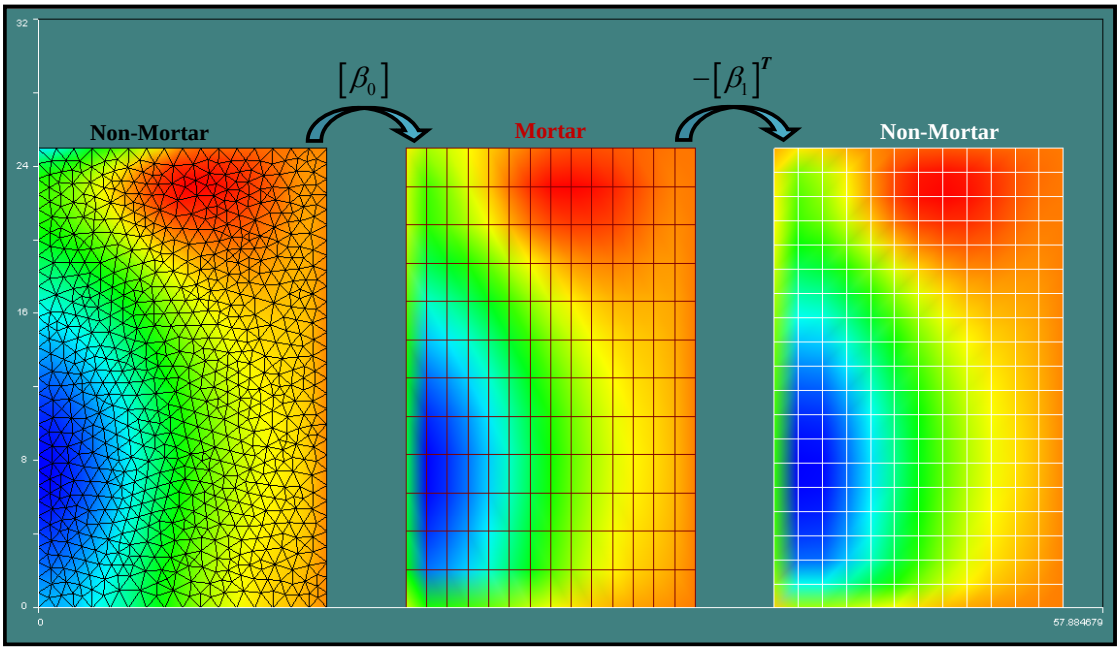

Figure 18: The projector action is exemplified by showing a parallel communication step.

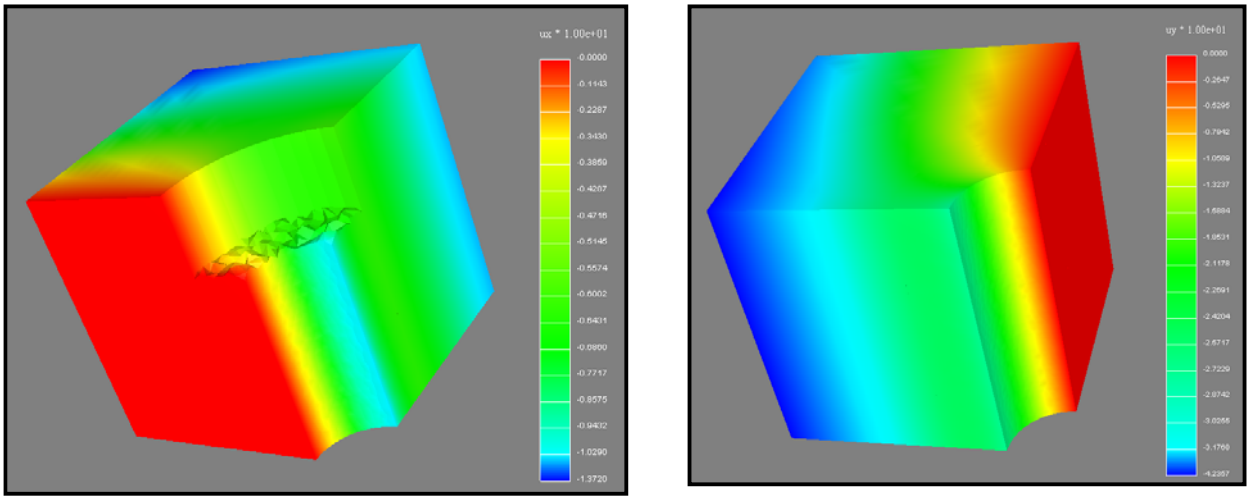

Figure 19: Results for u_x and u_y using the MFEM method in a near borehole problem. The figure on the left shows a cut (for visualization purposes) to better show the solution.

Fig. 19 shows the results obtained using the Mortar DD technique using the configuration depicted in Fig. 18. From this figures it is observed that a good match is obtained at the interface between the domains. This result suggests that it is possible to use this method to perform multiphysics simulations where a plastic zone develops in the vicinity of the wellbore, while poro-elasticity is assumed everywhere else.

Concluding Remarks

1. We have presented flow/geomechanics simulations using three of the main DDM, i.e., Dirichlet-Neumann, Neumann-Neumann and Mortar-FEM.
2. The implementation was successfully validated against the analytical solution of Mandel's problem.
3. Our formulation was applied to several practical cases ranging from near wellbore to full field simulations. In all situations considered, the DDM solutions show continuity across the interfaces between subdomains.
4. The serial-parallel approach seems to be appropriate to handle geomechanical problems involving different meshes for flow and mechanics as well as coupling parallel mechanistic codes with legacy flow simulators.
5. Near borehole simulation was implemented using general Mortar 3-D FEM method for elasticity producing good results in the sense that they are continuous across subdomain interfaces.

Future work

1. Extend the considered DD-schemes to parabolic problems; the serial-parallel implementation was an important step to achieve this goal in the very near future.
2. Apply Balancing Domain Decomposition to the NN-DDM.
3. Benchmark our code against academic and commercials simulators such as HYPLAS, FEAP and Abaqus.
4. Couple IPFA to major reservoir simulators, such as black oil and compositional flow models, via loose and/or iterative coupling with the serial-parallel or parallel-parallel architectures described in this paper.

Acknowledgments

The authors would like to thank ConocoPhillips for funding the project and permission to publish this paper. We want also to thank Mr. Omar Al Hinai for proof-reading the manuscript.

References

Abousleiman, Y., Cheng, A.H.D., Cui, L., Detournay, E., and Roegiers, J.C., 1996, Mandel's problem revisited: Geotechnique, v. 46, p. 187-195.

Babuska, I., 1973, Finite-Element Method With Lagrangian Multipliers: Numerische Mathematik, v. 20, p. 179-192.

Barber, J.R., 2002, Elasticity: New York, Kluwer Academic Publishers.

Belayneh, B.S.A.a.M., 2004, Elasto-plastic fracturing model for wellbore stability using non-penetrating fluids: Journal of Petroleum Science and Engineering, v. 45, p. 179-192.

Belgacem, F.B., 1999, The Mortar finite element method with Lagrange multipliers: Numer. Math., v. 84, p. 173-197.

Bernardi, C., Maday, Y., and Patera, A.T., 1994a, A new nonconforming approach to domain decomposition: the mortar element method, Nonlinear partial differential equations and their applications: Collège de France Seminar, vol. XI (Paris, 1989–1991), Longman Sci. Tech.

—, 1994b, A new nonconforming approach to domain decomposition: the mortar element method: Collège de France Seminar, vol. XI (Paris, 1989–1991), p. 13-51.
Bianco, M., Bilardi, G., Pesavento, F., Pucci, G., and Schrefler, B.A., 2003, A frontal solver tuned for fully coupled non-linear hygro-thermo-mechanical problems: International Journal for Numerical Methods in Engineering, v. 57, p. 1801-1818.
Biot, M., 1941, General theory of three-dimensional consolidation: J. Appl. Phys., v. 2, p. 155-164.
Bjorstad, P.E., and Widlund, O.B., 1986, Iterative Methods For The Solution Of Elliptic Problems On Regions Partitioned Into Substructures: Siam Journal on Numerical Analysis, v. 23, p. 1097-1120.
Booker, J.R., and Small, J.C., 1987, A Method of Computing The Consolidation Behavior of Layered Soils Using Direct Numerical Inversion of Laplace Transforms: International Journal for Numerical and Analytical Methods in Geomechanics, v. 11, p. 363-380.
Bourgat, J.F., Glowinsky, R., Tallec, P.L., and Vidrascu, M., 1988, Variational Formulation and Algorithm for Trace Operator in Domain Decomposition Calculations, Second International Symposium on Domain Decomposition Methods, SIAM, p. 3-16.
Charlez, P.A., 1991, Rock Mechanics, Volume I: Theoretical Fundamentals: France, Editions Technip.
—, 1999, The Concept of Mud Weight Window Applied to Complex Drilling, SPE-56758.
Chin, L.Y., Raghavan, R., and Thomas, L.K., 2000, Fully coupled geomechanics and fluid-flow analysis of wells with stress-dependent permeability: Spe Journal, v. 5, p. 32-45.
Coussy, O., 2004, Poromechanics: New York, Wiley.
Cowsar, L.C., Mandel, J., and Wheeler, M.F., 1995, Balancing Domain Decomposition For Mixed Finite-Elements: Mathematics of Computation, v. 64, p. 989-1015.
Dean, R.H., Gai, X., Stone, C.M., and Minkoff, S.E., 2006, A comparison of techniques for coupling porous flow and geomechanics: Spe Journal, v. 11, p. 132-140.
Destuynder, P., and Roux, F., 1988, A Parallel Solver for the Linear Elasticity Equations on a Composite Beam, *in* al., T.F.C.e., ed., Second International Symposium on Domain Decomposition Methods, SIAM, p. 314-320.
Ferronato, M., Castelletto, N., and Gambolati, G., 2010, A fully coupled 3-D mixed finite element model of Biot consolidation: Journal of Computational Physics, v. 229, p. 4813-4830.
Ferronato, M., Janna, C., and Gambolati, G., 2008, Mixed constraint preconditioning in computational contact mechanics: Computer Methods in Applied Mechanics and Engineering, v. 197, p. 3922-3931.
Fjaer, E., Holt, R.M., Horsrud, P., Raaen, A.M., and Risnes, R., 2008, Petroleum related rock mechanics: Hungary, Elsevier.
Flemisch, B., Puso, M.A., and Wohlmuth, B.I., 2005, A new dual mortar method for curved interfaces: 2D elasticity: International Journal for Numerical Methods in Engineering, v. 63, p. 813-832.
Fritz, A., Hueber, S., and Wohlmuth, B.I., 2004, A comparison of mortar and Nitsche techniques for linear elasticity: Calcolo, v. 41, p. 115-137.
Funaro, D., Quarteroni, A., and Zanolli, P., 1988, An Iterative Procedure With Interface Relaxation For Domain Decomposition Methods: Siam Journal on Numerical Analysis, v. 25, p. 1213-1236.
Gai, X., 2004, A Coupled Geomechanics and Reservoir Flow Model on Parallel Computers: Austin, The University of Texas.
Gassmann, F., 1951, Elastic waves through a packing of spheres: Geophysics v. 16, p. 673-685.
Gawin, D., Majoranna, C.E., Pesavento, F., and Schrefler, B.A., 1998, A fully coupled multiphase model of hydro-thermo-mechanical behaviour of concrete at high temperature, Fourth World Congress on Computational Mechanics, p. 1-19.
Geertsma, J., 1957, The effect of fluid pressure decline on volumetric changes of porous rocks: Trans. AIME, v. 210, p. 331-340.
—, 1973, LAND SUBSIDENCE ABOVE COMPACTING OIL AND GAS RESERVOIRS: Journal of Petroleum Technology, v. 25, p. 734-744.
Girault, V., Pencheva, G.V., Wheeler, M.F., and Wildey, T.M., 2009, Domain decomposition for linear elasticity with DG jumps and mortars: Computer Methods in Applied Mechanics and Engineering, v. 198, p. 1751-1765.
Glowinski, R., and Wheeler, M.F., 1988, Domain decomposition and mixed finite element methods for elliptic problems, *in* R. Glowinski, G.H.G., G.A. Meurant, J. Periaux, ed., First International Symposium on Domain Decomposition Methods for Partial Differential Equations, SIAM.
Gutierrez, M., Lewis, R.W., and Masters, I., 2001, Petroleum reservoir simulation coupling fluid flow and geomechanics: Spe Reservoir Evaluation & Engineering, v. 4, p. 164-172.
Hansbo, P., Lovadina, C., Perugia, I., and Sangalli, G., 2005, A Lagrange multiplier method for the finite element solution of elliptic interface problems using non-matching meshes: Numerische Mathematik, v. 100, p. 91-115.
Hauret, P., and Le Tallec, P., 2007, A discontinuous stabilized mortar method for general 3D elastic problems: Computer Methods in Applied Mechanics and Engineering, v. 196, p. 4881-4900.
Hauret, P., and Ortiz, M., 2006, BV estimates for mortar methods in linear elasticity: Computer Methods in Applied Mechanics and Engineering, v. 195, p. 4783-4793.
Kaasschieter, E.F., and Frijns, A.J.H., 2003, Squeezing a sponge: a three-dimensional solution in poroelasticity: Computational Geosciences, v. 7, p. 49-59.
Kim, C., Lazarov, R.D., Pasciak, J.E., and Vassilevski, P.S., 2001, Multiplier spaces for the mortar finite element method in three dimensions: Siam Journal on Numerical Analysis, v. 39, p. 519-538.

Kim, J., Tchelepi, H.A., and Juanes, R., 2009, Stability; Accuracy and Efficiency of Sequential Methods for Coupled Flow and Geomechanics, 2009 SPE Reservoir Simulation Symposium, Volume SPE 119084: The Woodlands, SPE.
Kim, K., Yi, D., and Lee, S., 2005, Mortar method for nonconforming finite elements: Applied Mathematics and Computation, v. 167, p. 650-669.
Lamichhane, B.P., Stevenson, R.P., and Wohlmuth, B.I., 2005, Higher order mortar finite element methods in 3D with dual lagrange multiplier bases: Numerische Mathematik, v. 102, p. 93-121.
Lewis, R.W., and Schrefler, B.A., 1998, The Finite Element Method in the Static and Dynamic Deformation and Consolidation of Porous Media: New York, John Wiley and Sons.
Liu, R., 2004, Discontinuous Galerkin Finite Element Solution for Poromechanics: Austin, The University of Texas.
Longuemare, P., Mainguy, M., Lemonnier, P., Onaisi, A., Gerard, C., and Koutsabeloulis, N., 2002, Geomechanics in reservoir simulation: Overview of coupling methods and field case study: Oil & Gas Science and Technology-Revue De L Institut Francais Du Petrole, v. 57, p. 471-483.
Maday, Y., and Magoules, F., 2006, Absorbing interface conditions for domain decomposition methods: A general presentation: Computer Methods in Applied Mechanics and Engineering, v. 195, p. 3880-3900.
Maday, Y., Mavriplis, C., and Patera, A.T., 1988, Nonconforming Mortar Element Methods: Application to Spectarl Discretizations, *in* al., T.F.C.e., ed., Second International Symposium on Domain Decomposition Methods, SIAM, p. 392-418.
Mandel, J., 1953, Consolidation des sols (etude mathhatique): Géotechnique, v. 3, p. 287-299.
Mandel, J., and Brezina, M., 1996, Balancing domain decomposition for problems with large jumps in coefficients: Mathematics of Computation, v. 65, p. 1387-1401.
Minkoff, S.E., Stone, C.M., Bryant, S., Peszynska, M., and Wheeler, M.F., 2003, Coupled fluid flow and geomechanical deformation modeling: Journal of Petroleum Science and Engineering, v. 38, p. 37-56.
Muller, A.L., Jr, E.d.A.V., Vaz, L.E., and Goncalves, C.J., 2009, Borehole stability analysis considering spatial variability and poroelastoplasticity: International Journal of Rock Mechanics and Mining Sciences, v. 46, p. 90-96.
Pao, W.K.S., Lewis, R.W., and Masters, I., 2001, A fully coupled hydro-thermo-poro-mechanical model for black oil reservoir simulation: International Journal for Numerical and Analytical Methods in Geomechanics, v. 25, p. 1229-1256.
Phillips, P.J., 2005, Finite Element Methods in Linear Poroelasticity: Theoretical and Computational Results: Austin, The University of Texas
Phillips, P.J., and Wheeler, M.F., 2007a, A coupling of mixed and continuous Galerkin finite element methods for poroelasticity I: the continuous in time case: Computational Geosciences, v. 11, p. 131-144.
—, 2007b, A coupling of mixed and continuous Galerkin finite element methods for poroelasticity II: the discrete-in-time case: Computational Geosciences, v. 11, p. 145-158.
Puso, M.A., 2004, A 3D mortar method for solid mechanics: International Journal for Numerical Methods in Engineering, v. 59, p. 315-336.
Quarteroni, A., and Valli, A., 1999, Domain Decomposition Methods for Partial Differential Equations: Oxford Oxford University Press.
Rice, J.R., and Cleary, M.P., 1976, SOME BASIC STRESS DIFFUSION SOLUTIONS FOR FLUID-SATURATED ELASTIC POROUS-MEDIA WITH COMPRESSIBLE CONSTITUENTS: Reviews of Geophysics, v. 14, p. 227-241.
Sandhu, R.S., and Wilson, E.L., 1969, Finite element analysis of seepage in elastic media: J. Eng. Mech. Div., ASCE, v. 95, p. 641-652.
Santarelli, F.J., Dahen, D., Baroudi, H., and Sliman, K.B., 1992, Mechanisms of Borehole Instability in Heavily Fractured Rock Media: Int. J. Rock Mech. Min. Sci. and Geomech. Abstr., v. 29, p. 457-467.
Settari, A., and Walters, D.A., 2001, Advances in coupled geomechanical and reservoir modeling with applications to reservoir compaction: Spe Journal, v. 6, p. 334-342.
Shao, J.F., 1997, A numerical solution for a thermo-hydro-mechanical coupling problem with heat convection: International Journal of Rock Mechanics and Mining Sciences, v. 34, p. 163-166.
Souza-Neto, E.A.d., Peric, D., and Owen, D.R.J., 2008, Computational Methods for Plasticity: Theory and Applications: United Kingdom, John Wiley and Sons Ltd.
Stavroulakis, G.M., and Papadrakakis, M., 2009, Advances on the domain decomposition solution of large scale porous media problems: Computer Methods in Applied Mechanics and Engineering, v. 198, p. 1935-1945.
Terzaghi, K., 1923, Die Berechnung der Durchlassigkeitsziffer des Tones aus dem Verlauf der hydrodynamischen Spannungserscheinungen: Sitzung Berichte. Akadamie der Wissenschaften, Wien Mathematisch-Naturwissenschaftliche Klasse, Abteilung IIa, v. 132, p. 105-124.
—, 1943, Theoretical Soil Mechanics: New York, Wiley.
Toselli, A., and Widlund, O.B., 2004, Domain Decomposition Methods: Algorithms and Theory},
publisher Springer.
Turska, E., and Schrefler, B.A., 1993, ON CONVERGENCE CONDITIONS OF PARTITIONED SOLUTION PROCEDURES FOR CONSOLIDATION PROBLEMS: Computer Methods in Applied Mechanics and Engineering, v. 106, p. 51-63.

Turska, E., Wisniewski, K., and Schrefler, B.A., 1994, ERROR PROPAGATION OF STAGGERED SOLUTION PROCEDURES FOR TRANSIENT PROBLEMS: Computer Methods in Applied Mechanics and Engineering, v. 114, p. 177-188.

Wheeler, M.F., 1978, ELLIPTIC COLLOCATION-FINITE ELEMENT METHOD WITH INTERIOR PENALTIES: Siam Journal on Numerical Analysis, v. 15, p. 152-161.

Wohlmuth, B.I., 2000, A mortar finite element method using dual spaces for the Lagrange multiplier: Siam Journal on Numerical Analysis, v. 38, p. 989-1012.

Yin, S.D., Dusseault, M.B., and Rothenburg, L., 2009, Thermal reservoir modeling in petroleum geomechanics: International Journal for Numerical and Analytical Methods in Geomechanics, v. 33, p. 449-485.

Zienkiewicz, O.C., Humpheson, C., and Lewis, R.W., 1977, A unified approach to soil mechanics problems including plasticity and visco-plasticity, *in* Gudehus, G., ed., Finite Elements in Geomechanics, Wiley, New York, p. 151–-177.

Zienkiewicz, O.C., and Shiomi, T., 1984, Dynamic behavior of saturated porous media: the generalized Biot formulation and its numerical solution: Int. J. Numer. Anal. Methods Geomech., v. 8, p. 71-96.